Consistent Large Eddy Simulation of a temporal mixing layer laden with evaporating drops. Part II: *A priori* modeling

By NORA A. OKONG'O and JOSETTE BELLAN †

Jet Propulsion Laboratory, California Institute of Technology, Pasadena, CA 91109-8099, USA

(Received 18 July 2002)

Large Eddy simulation (LES) models are presented and evaluated on a database obtained from Direct Numerical Simulation (DNS) of a three-dimensional temporal mixing layer with evaporating drops. The gas-phase equations are written in an Eulerian frame for two perfect gas species (carrier gas and vapor emanating from the drops), while the liquid-phase equations are written in a Lagrangian frame. The DNS database (described and analyzed in Part I) consists of transitional states attained by layers with different initial Reynolds numbers and initial liquid-phase mass loadings. The LES models evaluated at these transitional states are of two types: those for the filtered source terms representing the effect of the drops on the filtered flow field, and those for the subgrid scale (SGS) fluxes arising from filtering the convective terms in the DNS equations. The filtered source term models are applicable to LES in which the grid is coarser than the DNS grid and, consistently, the DNS physical drops are represented by fewer drops, called 'computational' drops in the LES context. Because the unfiltered flow field is required for the calculation of drop-based quantities that enter the computation of the source terms,

† Author for correspondence: Josette.Bellan@jpl.nasa.gov

but this unfiltered flow field would not be available in LES, various approximations were attempted for it, namely, the filtered flow field and the filtered flow field augmented by corrections based on the SGS variances. All of the filtered source term models were found to overestimate filtered source terms, with the relative error of modeling the unfiltered flow field compared to the error of using computational drops showing a complex dependence on filter width and number of computational drops. For modeling the SGS fluxes, constant-coefficient Smagorinsky, Gradient and Scale-Similarity models were assessed and calibrated on the DNS database, with the Gradient and Scale-Similarity models showing excellent correlation with the SGS quantities they are used to replicate. An *a posteriori* study is proposed to evaluate the impact of the studied models on the flow field development, so as to definitively assess their suitability for LES with evaporating drops.

---

1. Introduction

The Large Eddy Simulation (LES) methodology was conceived for single-phase (SP) flows to decrease computational costs through restricting the resolution to that of the large scales and including the effect of the small scales through models. The LES equations are obtained by spatially filtering the Direct Numerical Simulation (DNS) equation set, as DNS are simulations which compute the entire range of scales typical of turbulent flows. For compressible multi-species flows, this filtering process introduces unresolved momentum, energy and species subgrid scale (SGS) fluxes. (For incompressible SP LES, only the momentum SGS fluxes, usually referred to as SGS stresses, arise.) Therefore, for SP flows, the necessary SGS models consist of expressions relating the SGS fluxes to the resolved variables. For two-phase (TP) flows with evaporating (liquid) drops, the

situation is more complicated because the filter volume contains drops. Assuming that the drops are small enough to be treated as point sources, their evolution depends on the gas-phase flow field, and in turn they affect the gas phase by acting as sources of mass, momentum and energy. Consistency in the goal of decreasing computational costs dictates that not only must the flow resolution be decreased in LES with respect to DNS, but the same concept also must be applied to the ensemble of drops. That is, in LES the drops should not be the genuine drops of DNS, but instead should be 'computational' drops representing the effect of several genuine drops. Therefore, TP LES requires modeling both the effect of the flow field on the drops (through the drop far-field), and that of the drops on the flow field (through filtered source terms).

In Part I of this investigation (Okong'o & Bellan (2002)), we created the DNS database that will here be used in developing and assessing these models, we derived the LES equations, and then we computed the budgets of these equations and assessed some simplifying assumptions on the filtered DNS flow field. That analysis established the need for accurate models of the filtered source terms and of the SGS fluxes. In the present study, we seek to introduce a consistent two-phase flow LES methodology wherein both the number of grid points and that of tracked drops is reduced compared to DNS, and to develop the necessary models for the filtered source terms and the SGS fluxes. SGS TP flow models that treated the drop contribution but did not reduce the size of the drop ensemble or consider the effect of the drops on the flow field were presented by Miller & Bellan (2000) and Okong'o & Bellan (2000). Some of these models shall be extended so as to calculate the filtered source terms from the filtered flow field and the reduced drop ensemble. Concerning the SGS fluxes, the focus will be on adapting and calibrating for TP flows, with phase change, models originally developed for incompressible SP LES. The SGS models we shall consider are the Smagorinsky (see Smagorinksy (1993)), Scale-

Similarity (Bardina *et al.* (1980)) and Gradient (Clark *et al.* (1979)) models. The application of these models to compressible flows is usually made through density-weighting. However, unlike incompressible flows for which only the momentum equation along with the pressure perturbation from a reference are considered, compressible flows require computation of the physical pressure through the equation of state as well as solution of the energy equation. The required models depend on the form of the energy equation that is used (e.g. Erlebacher *et al.* (1992), Fureby (1996), Martin *et al.* (2000)). In the present situation, the vapor emanating from the drops requires the consideration of yet another equation to describe species conservation. The thermodynamic variables (density, pressure, composition, energy, temperature) are coupled through the equation of state, as well as through the heat and mass fluxes appearing in the energy and species equations. Therefore, appropriate modeling of the momentum, energy and species SGS fluxes must be carefully assessed.

This paper is organized as follows: In § 2 we summarize the DNS equations which constitute a set comprising coupled conservation equations for the gas phase and liquid phase. The coupling describing the interaction between the two phases is provided in the gas-phase conservation equations by source terms. These equations were used to generate the DNS database, as detailed by Okong'o & Bellan (2002), which is summarized in § 2.5. The LES equations derived in Okong'o & Bellan (2002) are presented in § 3, and the terms requiring modeling are identified. Models for the filtered source terms appearing in the LES equations are investigated in § 4, while several constant-coefficient SGS models are proposed and calibrated in § 5. Finally, conclusions and further discussions are presented in § 6.

2. DNS equations

The detailed DNS equations along with the justification of the assumptions embodied in them were described in Part I (Okong'o & Bellan (2002)), based on the formulation of Miller & Bellan (1999). Here, we present only those aspects relevant to the LES methodology designed to replicate the DNS large scales. The governing equations are formulated in an Eulerian frame for the gas phase and a Lagrangian frame for the drops. The gas phase consists of two species which are the carrier gas and the vapor evolving from the drops. The drops are treated as point sources of mass, momentum and energy for the gas phase; this treatment is justified by the dilute (i.e. volumetrically small, $O(10^{-3})$) loading and the size of each particle being much smaller than the Kolmogorov scale.

2.1. *Gas phase equations*

We define the vector of gas-phase conservative variables $\phi = \{\rho, \rho u_i, \rho e_t, \rho Y_V\}$ and denote the DNS flow field as ϕ, where ρ is the density, u_i is the velocity in the x_i coordinate direction, e_t is the total energy and Y_V is the vapor (subscript V) mass fraction (the carrier gas, subscript C, mass fraction is Y_C; $Y_C + Y_V = 1$). The gas-phase conservation equations are:

$$\frac{\partial \rho}{\partial t} + \frac{\partial (\rho u_j)}{\partial x_j} = S_I, \tag{2.1}$$

$$\frac{\partial (\rho u_i)}{\partial t} + \frac{\partial (\rho u_i u_j)}{\partial x_j} = -\frac{\partial p}{\partial x_i} + \frac{\partial \sigma_{ij}}{\partial x_j} + S_{II,i}, \tag{2.2}$$

$$\frac{\partial (\rho e_t)}{\partial t} + \frac{\partial (\rho e_t u_j)}{\partial x_j} = -\frac{\partial (p u_j)}{\partial x_j} - \frac{\partial q_j}{\partial x_j} + \frac{\partial (\sigma_{ij} u_i)}{\partial x_j} + S_{III}, \tag{2.3}$$

$$\frac{\partial (\rho Y_V)}{\partial t} + \frac{\partial (\rho Y_V u_j)}{\partial x_j} = -\frac{\partial j_{Vj}}{\partial x_j} + S_I, \tag{2.4}$$

$$\frac{\partial (\rho Y_C)}{\partial t} + \frac{\partial (\rho Y_C u_j)}{\partial x_j} = -\frac{\partial j_{Cj}}{\partial x_j}, \tag{2.5}$$

where S_I, $S_{II,i}$ and S_{III} are source terms due to the interaction with the drops. The thermodynamic variables, to be computed from ϕ, are the internal energy ($e = e_t -$

$u_i u_i/2$), the pressure (p), the temperature (T) and the enthalpy ($h = e + p/\rho$). We assume perfect gases, for which the pressure is

$$p(\phi) = \rho R(\phi) T(\phi), \tag{2.6}$$

where $R = R_V Y_V + R_C Y_C$, $R_V = R_u/m_V$, $R_C = R_u/m_C$, R_u is the universal gas constant and m_C and m_V are the molar weights of the carrier gas and vapor respectively. We further assume calorically perfect gases (constant specific heats), so that

$$h(\phi) = C_p(\phi) T(\phi) + h_V^0 Y_V, \tag{2.7}$$

where $C_p = C_{p,V} Y_V + C_{p,C} Y_C$, $C_{p,C} = C_{p,C}(T^0)$ and $C_{p,V} = C_{p,V}(T^0)$ and h_V^0 is the reference vapor enthalpy at (T^0, p^0) obtained from integration or tables, which accounts for the enthalpy difference between the vapor and carrier gas at the reference conditions.

For (2.1)–(2.5), we also specify: the viscous stress,

$$\sigma_{ij}(\phi) = 2\mu \left(S_{ij} - \frac{1}{3} S_{kk} \delta_{ij} \right), \tag{2.8}$$

where μ is the viscosity and

$$S_{ij}(\phi) = \frac{1}{2} \left(\frac{\partial u_i}{\partial x_j} + \frac{\partial u_j}{\partial x_i} \right) \tag{2.9}$$

is the rate of strain; the vapor mass flux,

$$j_{Vj}(\phi) = \rho Y_V V_{Vj}(\phi) = -\rho Y_V \left[\frac{D}{Y_V} \frac{\partial Y_V}{\partial x_j} + Y_C \left(Y_V + Y_C \frac{m_V}{m_C} \right) \left[\frac{m_C}{m_V} - 1 \right] \frac{D}{p(\phi)} \frac{\partial p(\phi)}{\partial x_j} \right], \tag{2.10}$$

where thermal diffusion effects have been neglected, V_{Vj} is the vapor diffusion velocity, and D is the diffusion coefficient; the carrier gas mass flux

$$j_{Cj}(\phi) = \rho Y_V V_{Cj}(\phi) = -j_{Vj}(\phi) \tag{2.11}$$

and the heat flux,

$$q_j(\phi) = -\lambda \frac{\partial T(\phi)}{\partial x_j} + (h_V(\phi) - h_C(\phi)) j_{Vj}(\phi), \tag{2.12}$$

where λ is the thermal conductivity. In (2.8), (2.10) and (2.12), μ, D and λ are assumed constant, and may be defined through the Prandtl and Schmidt numbers, $\mathrm{Pr} = \mu C_p/\lambda$ and $Sc = \mu/(\rho D)$.

2.2. *Drop (liquid-phase) equations*

The equations describing the drop evolution have been presented in detail by Miller & Bellan (1999) and only their essence is presented here. We define $Z = \{X_i, v_i, T_d, m_d\}$ as the drop field with position X_i, velocity v_i, temperature T_d, and mass m_d. Under the assumptions stated previously, the evolution equations for each drop, in a Lagrangian frame, are:

$$\frac{dX_i}{dt}(Z) = v_i, \tag{2.13}$$

$$\frac{dv_i}{dt}(\psi_f, Z) = \frac{1}{m_d} F_i(\psi_f, Z), \tag{2.14}$$

$$\frac{dT_d}{dt}(\psi_f, \psi_s, Z) = \frac{1}{m_d C_L}\left[Q(\psi_f, Z) + \dot{m}_d(\psi_f, \psi_s, Z) L_V(Z)\right], \tag{2.15}$$

$$\frac{dm_d}{dt}(\psi_f, \psi_s, Z) = \dot{m}_d(\psi_f, \psi_s, Z), \tag{2.16}$$

where F_i is the drag force, Q is the heat flux, $\dot{m}_d$ is the evaporation rate, and C_L is the heat capacity of the drop liquid. L_V is the latent heat of vaporization, which, for calorically perfect gases, is a linear function of temperature, $L_V = h_V^0 - (C_L - C_{p,V})T_d$. The drop evolution depends on the gas-phase primitive variables, $\psi(\phi) = \{u_i, T, Y_V, p\}$, whose value at the drop surface (subscript s) and at the drop far-field (subscript f) enter the calculation. The far-field variables are taken as the gas-phase primitive variables interpolated to the drop locations. The detailed expressions for F_i, Q, and $\dot{m}_d$ involve validated point-drop correlations which are based on Stokes drag, with particle time constant $\tau_d = \rho_L d^2/(18\mu)$, where ρ_L is the density of the liquid and d is the drop

diameter ($m_d = \rho_L \pi d^3/6$):

$$F_i(\psi_f, Z) = \frac{m_d}{\tau_d} f_1(u_{i,f} - v_i), \tag{2.17}$$

$$Q(\psi_f, Z) = \frac{m_d}{\tau_d} \frac{Nu}{3\,\mathrm{Pr}} C_{p,f} f_2 (T_f - T_d), \tag{2.18}$$

$$\dot{m}_d(\psi_f, Z) = -\frac{m_d}{\tau_d} \frac{Sh}{3Sc} \ln\left[1 + B_M\right]. \tag{2.19}$$

In (2.17), f_1 is an empirical correlation to correct the Stokes drag for finite drop Reynolds numbers

$$f_1 = \frac{1 + 0.0545\,\mathrm{Re}_{sl} + 0.1\,\mathrm{Re}_{sl}^{1/2}\left(1 - 0.03\,\mathrm{Re}_{sl}\right)}{1 + a\left|\mathrm{Re}_b\right|^b}, \tag{2.20}$$

$$a = 0.09 + 0.077\exp\left(-0.4\,\mathrm{Re}_{sl}\right), \qquad b = 0.4 + 0.77\exp\left(-0.04\,\mathrm{Re}_{sl}\right), \tag{2.21}$$

based on the slip Reynolds number $\mathrm{Re}_{sl} = |u_{i,f} - v_i|\,\rho d/\mu$ where $u_{i,f} - v_i$ is the slip velocity, and on the blowing Reynolds number $\mathrm{Re}_b = U_b \rho d/\mu$ where U_b is the blowing velocity obtained from the mass conservation relation at the drop surface, $\dot{m}_d = -\pi \rho d^2 U_b$. The correlation of (2.20) is valid for the ranges $0 \leqslant \mathrm{Re}_{sl} \leqslant 100$ and $0 \leqslant \mathrm{Re}_b \leqslant 10$. In (2.18), $C_{p,f} = C_{p,V} Y_{V,f} + C_{p,C} Y_{C,f}$ and $f_2 = \beta/(e^\beta - 1)$, where $\beta = -1.5\,\mathrm{Pr}\,\dot{m}_d \tau_d / m_d$ is constant for drops obeying the classical 'd^2 law' (Williams (1965)). In (2.19), the mass transfer number is $B_M = (Y_{V,s} - Y_{V,f})/(1 - Y_{V,s})$ where the surface vapor mass fraction, $Y_{V,s}$, is calculated directly from the mole fraction, $X_{V,s}$, which is obtained by equating the vapor and liquid fugacities at the surface (i.e. $X_{V,s} p_s = p_{sat}$; also $p_s = p_f$), where the saturation pressure, p_{sat}, is provided by the Clausius-Clapeyron relation. This leads to

$$X_{V,s} = \frac{p_{atm}}{p_s} \exp\left[\frac{L_V}{R_V}\left(\frac{1}{T_{B,L}} - \frac{1}{T_d}\right)\right], \qquad Y_{V,s} = \frac{X_{V,s}}{X_{V,s} + \left(1 - X_{V,s}\right) m_C/m_V}, \tag{2.22}$$

where p_{atm}=1 atm and $T_{B,L}$ is the liquid saturation temperature at p_{atm} (i.e. the normal boiling temperature). Finally, the Nusselt, Nu, and Sherwood, Sh, numbers appearing in (2.18) and (2.19) are empirically modified for convective corrections to heat and mass

transfer based on the Ranz-Marshall correlations

$$Nu = 2 + 0.552\ \mathrm{Re}_{sl}^{1/2}\,(\mathrm{Pr})^{1/3}\,, \qquad Sh = 2 + 0.552\,\mathrm{Re}_{sl}^{1/2}\,(Sc)^{1/3}\,. \tag{2.23}$$

Except for τ_d, which depends on μ, (2.17)–(2.19) depend essentially on ratios of transport properties through non-dimensional numbers. Therefore, the value of τ_d and thus for a given liquid and drop size, the value of μ determines the interaction time between drops and gas.

2.3. *Source terms*

As in Miller & Bellan (1999), each drop acts as a point source of mass, momentum and energy for the gas phase, with the drop source vector

$$S_d\,(\psi_f, Z) = \{S_{I,d}, S_{II,i,d}, S_{III,d}\}\,, \tag{2.24}$$

$$S_{I,d} = -\dot{m}_d, \tag{2.25}$$

$$S_{II,i,d} = -\left[F_i + \dot{m}_d v_i\right], \tag{2.26}$$

$$S_{III,d} = -\left[F_i v_i + Q + \dot{m}_d\left(\tfrac{1}{2}v_i v_i + h_{V,s}\right)\right], \tag{2.27}$$

where $h_{V,s} = C_{p,V}T_d + h_V^0$ is the vapor enthalpy at the drop surface. The drop sources in the Lagrangian frame must be reconstructed in the Eulerian frame to obtain the gas-phase source vector S which contains the terms in (2.1)–(2.4), $S\,(\psi_f, Z) = \{S_I, S_{II,i}, S_{III}\}$. As in Miller & Bellan (1999), we use

$$S\,(\psi_f, Z) = \sum_{\alpha} \frac{w_\alpha}{V}\left[S_d\,(\psi_f, Z)\right]_\alpha\,, \tag{2.28}$$

where the summation is over all drops α residing within a local numerical discretization volume, V, and the geometrical weighting factor, w_α, is used to distribute the individual drop contributions to the eight nearest neighbor surrounding grid points (i.e. corners of the computational volume V) proportionally to the drop distance from those nodes.

These source terms are then minimally 'smoothed' using a conservative operator so as to retain numerical stability of the Eulerian gas-phase fields.

2.4. *Flow configuration and numerical procedure*

The mixing layer geometric configuration is illustrated in figure 1 where the streamwise (x_1), the cross-stream (x_2), and the spanwise (x_3), coordinates are shown, and the domain lengths are L_1, L_2 and L_3 in each direction. Periodic boundary conditions are used in the x_1 and x_3 directions, and adiabatic slip wall conditions (see Poinsot & Lele (1992)) are employed for the x_2 boundaries. The free-stream velocity $U_0 = M_{c,0}a_{C,0}$ is calculated from a specified value of the convective Mach number $M_{c,0}$ based on the carrier gas initial speed of sound $a_{C,0} = \sqrt{R_C T_{C,0} C_{p,C}/C_{v,C}}$ where $T_{C,0}$ is the initial uniform temperature of the carrier gas at the initial uniform pressure; the carrier gas is the sole initial species in the gas phase. The initial vorticity thickness is $\delta_{\omega,0} = \delta_\omega(0)$ where $\delta_\omega(t) = \Delta U_0/(\partial\langle u_1\rangle/\partial x_2)_{\max}$ with the brackets $\langle\rangle$ denoting averaging over homogeneous (x_1, x_3) planes and the velocity difference across the layer is $\Delta U_0 = 2U_0$; the initial mean streamwise velocity has an error-function profile. The specified value of the initial Reynolds number, $\mathrm{Re}_0 = \rho_0 \Delta U_0 \delta_{\omega,0}/\mu$, where ρ_0 is the initial gas density, is used to calculate μ. The thermal conductivity and diffusivity are then computed using this value of μ and specified values of Prandtl and Schmidt numbers of 0.697 (the Lewis number is unity). All thermophysical properties are the same as those employed in the simulations of Miller & Bellan (2000) using air as the carrier gas and decane as the drop liquid.

To promote layer growth, the layer is initially perturbed so as to induce roll-up and pairing. The perturbations, described in Miller & Bellan (1999), follow Moser & Rogers (1991) in specifying spanwise and streamwise vorticity fluctuations, with streamwise and spanwise wavelengths in the x_1 and x_3 directions of $\lambda_1 = 7.29\delta_{\omega,0}$ and $\lambda_3 = 0.6\lambda_1$. For

all the simulations performed herein, $L_1 = 0.2$ m, $L_1 = 4\lambda_1$, $L_2 = 1.1L_1$ and $L_3 = 4\lambda_3$. The relative amplitudes of the forcing perturbations with respect to the circulations are 10% and 2.25% in the spanwise and streamwise directions, respectively.

The drops are initially distributed randomly throughout the $x_2 < 0$ domain with specified temperature, velocity, number density and size distribution. Initially, all the drops have the same temperature, $T_{d,0}$, and have the same velocity as the gas phase at their location. The mean number density profile is smoothed near the center-line, $x_2 = 0$, using an error function profile. The drop size distribution is initially specified through the drop Stokes number $St = \tau_d \Delta U_0/\delta_{\omega,0}$ whose initial distribution is Gaussian with mean 3 and standard deviation 0.5. The number of drops is determined by the initial mass loading ML_0 (initial ratio of mass of liquid to mass of carrier gas in drop-laden part of domain).

2.5. *DNS database*

The above DNS equations were solved numerically using a fourth-order explicit Runge-Kutta temporal integration for time derivatives and eight-order central finite differences with tenth-order filtering for spatial derivatives (Kennedy & Carpenter (1994)). A fourth-order Lagrange interpolation procedure was used to obtain gas-phase variable values at the drop locations. The DNS endeavor was undertaken to achieve several transitional states that could be further analyzed for *a priori* turbulence modeling. DNS initial conditions are listed in Table 1. Detailed characterization of these simulations, including the adequacy of the resolution and flow visualizations of the $\mathrm{Re}_0 = 600$ transitional states are described in Part I (Okong'o & Bellan (2002)). In the present paper, *a priori* analysis will be restricted to SP600 and TP600a2, with the intention of 'blind' testing the models thus obtained on the other cases on an *a posteriori* basis (Part III of this study).

3. LES equations

The LES uses a mathematical description similar to that of DNS, i.e. Eulerian for the gas phase and Lagrangian for the liquid phase. Drops tracked in the LES will follow the DNS evolution equations presented in § 2.2; however, the LES may use computational (defined in § 4.2) rather than physical drops. The gas-phase LES equations are derived by spatially filtering the gas-phase DNS equations described in § 2.1. The filtering operation is defined as

$$\bar{\psi}(\vec{x}) = \int_{V_f} \psi(\vec{y})\, G(\vec{x}-\vec{y})\, d\vec{y}, \tag{3.1}$$

where G is the filter function, with the property that $\bar{1} = 1$, and V_f is the filtering volume. In this study, G is a top-hat (box) filter, and therefore $\bar{\psi}$ is simply the volume-average. The Favre (density-weighted) filtering is defined as $\tilde{\psi} = \overline{\rho\psi}/\bar{\rho}$. We also assume that filtering and differentiation commute, which is correct except near boundaries (because the size of the filtering volume decreases as the boundary is approached).

After incorporating various simplifying assumptions (see Okong'o & Bellan (2002)), the LES equations become

$$\frac{\partial \bar{\rho}}{\partial t} + \frac{\partial(\bar{\rho}\tilde{u}_j)}{\partial x_j} = \bar{S}_I, \tag{3.2}$$

$$\frac{\partial(\bar{\rho}\tilde{u}_i)}{\partial t} + \frac{\partial(\bar{\rho}\tilde{u}_i\tilde{u}_j)}{\partial x_j} = -\frac{\partial\left[p\left(\bar{\phi}\right)\right]}{\partial x_i} + \frac{\partial\sigma_{ij}\left(\bar{\phi}\right)}{\partial x_j} + \bar{S}_{II,i} - \frac{\partial(\bar{\rho}\tau_{ij})}{\partial x_j}, \tag{3.3}$$

$$\begin{aligned}\frac{\partial(\bar{\rho}\tilde{e}_t)}{\partial t} + \frac{\partial(\bar{\rho}\tilde{e}_t\tilde{u}_j)}{\partial x_j} = &-\frac{\partial\left[p\left(\bar{\phi}\right)\tilde{u}_j\right]}{\partial x_j} - \frac{\partial q_j\left(\bar{\phi}\right)}{\partial x_j} + \frac{\partial\left[\sigma_{ij}\left(\bar{\phi}\right)\tilde{u}_i\right]}{\partial x_j} + \bar{S}_{III} \\ &- \frac{\partial\bar{\rho}\zeta_j}{\partial x_j} - \frac{\partial}{\partial x_j}\left[\bar{\rho}\tau_{ij}\tilde{u}_i\right],\end{aligned} \tag{3.4}$$

$$\frac{\partial\left(\bar{\rho}\tilde{Y}_V\right)}{\partial t} + \frac{\partial\left(\bar{\rho}\tilde{Y}_V\tilde{u}_j\right)}{\partial x_j} = -\frac{\partial j_{Vj}\left(\bar{\phi}\right)}{\partial x_j} + \bar{S}_I - \frac{\partial(\bar{\rho}\eta_j)}{\partial x_j}, \tag{3.5}$$

where the SGS fluxes are given by

$$\tau_{ij} = \widetilde{u_i u_j} - \tilde{u}_i\tilde{u}_j, \quad \zeta_j = \widetilde{hu_j} - \tilde{h}\tilde{u}_j, \quad \eta_j = \widetilde{Y_V u_j} - \tilde{Y}_V\tilde{u}_j. \tag{3.6}$$

The notation $f\left(\bar{\phi}\right)$ denotes a function of the filtered flow field, $\bar{\phi}$, that has the same functional form as in the DNS but is in general different from its filtered counterpart $\overline{f\left(\phi\right)}$. (The replacement of $\overline{f\left(\phi\right)}$ by $f\left(\bar{\phi}\right)$ that is implicit in (3.2)–(3.5) was found by Okong'o & Bellan (2002) to be generally valid for the flow fields in this study.)

From (3.1), the filtered source terms ($\bar{S} = \left\{\bar{S}_I, \bar{S}_{II,i}, \bar{S}_{III}\right\}$) are properly interpreted by considering a drop located at $\vec{X}$ within the filtering volume V_f and its contribution within that volume

$$\bar{S}\left(\vec{x}\right) = \int_{V_f} S_d \delta\left(\vec{y} - \vec{X}\right) G\left(\vec{x} - \vec{y}\right) d\vec{y}, \tag{3.7}$$

where $S_d \delta\left(\vec{y} - \vec{X}\right)$ is the point-source contribution from the drop and δ is the delta function. For G being a top-hat filter, the filtered source term is a volume-average over the drops β within the filtering volume

$$\bar{S}\left(\psi_f, Z\right) = \frac{1}{V_f} \sum_{\beta} \left[S_d\left(\psi_f, Z\right)\right]_{\beta}, \tag{3.8}$$

where S_d was previously defined in (2.24). (Note that $\bar{S}$ is not obtained by filtering the DNS S obtained through (2.28).)

Equations (3.2) – (3.5) for $\bar{\phi}$ contain terms that cannot be computed directly from $\bar{\phi}$ and that therefore need to be modeled, namely, (1) the filtered source terms ($\bar{S}_I$, $\bar{S}_{II,i}$, $\bar{S}_{III}$) and (2) the SGS fluxes (τ_{ij}, ζ_j, η_j).

4. Models for filtered source terms

In LES of TP flow with evaporating drops, the effect of the drops on the gas phase occurs through the filtered drop source terms ($\bar{S}$). Two modeling issues arise in computing $\bar{S}$. First, in calculating $\bar{S}$ through (3.8), the source effect of each drop (S_d) depends on both the drop state (Z) and the unfiltered variables at the drop far-field (ψ_f). However, in LES, ψ_f is not available and must be modeled from the filtered flow field ($\bar{\phi}$). Second,

for the gas phase, the resolution requirements for LES can be reduced compared to DNS because in LES only the large scales need to be resolved. In a similar spirit, the computational demands for the liquid phase can be diminished by simulating a reduced drop field, here denoted $\bar{Z}$, in which case $\bar{S}$ now needs to be modeled from $\bar{Z}$. The proposed models for $\bar{S}$ address the two issues just elaborated, namely, the calculation of ψ_f from $\bar{\phi}$ and the reduction of the number of tracked drops. Using the available DNS database, such models can be compared *a priori* against the 'exact' filtered source terms, i.e. $\bar{S}(\psi_f, Z)$ calculated from the actual unfiltered flow field and the full drop field. When analyzing the DNS database, the issue of the reduced drop field may be separated from that of unfiltered variable modeling by calculating filtered source term models using the actual unfiltered variables but with the reduced drop field, or using the modeled unfiltered variables along with the full drop field. By considering an 'ideal' unfiltered variable model that is the same as the actual unfiltered variables, and that would thereby accurately incorporate the gas-phase SGS effects, we can designate all the filtered source term models according to the underlying unfiltered variable models, which are described next.

4.1. *Models of the unfiltered gas-phase variables at drop locations*

A requirement to model the filtered source terms is the determination of the gas-phase quantities to be used in computing the source term contribution of the individual drops. In the modeling proposed here, the drop source terms (S_d) will be computed using the DNS relations (see § 2.2), which require the knowledge of the drop far-field. In the DNS, the flow field (ϕ) is computed at the grid points and the drop far-field (ψ_f) is computed at drop locations. The DNS procedure to obtain ψ_f from ϕ can be conceptualized as $\psi(\phi) \xrightarrow{\mathcal{I}} \psi_f$, where $\psi(\phi)$ denotes the functional dependence between primitive (ψ) and conservative (ϕ) variables which is used to compute primitive variables at the grid points

and $\mathcal{I}$ denotes the interpolation process from grid points to drop locations. The LES requires computing from the filtered flow field $(\bar{\phi})$ a model (subscript m) for the drop far-field, denoted $\psi_{f,m}$, which necessarily entails a reconstruction process $\mathcal{R}^*$. Defining the filtered gas-phase primitive variables as $\tilde{\psi} = \left\{\tilde{u}_i, \tilde{T}, \tilde{Y}_V, \bar{p}\right\}$, then consistent with the gas-phase equations (see § 3), $\tilde{\psi}\left(\bar{\phi}\right)$ takes the same form as $\psi\left(\phi\right)$. Two possible LES procedures for calculating $\psi_{f,m}$ are: (1) $\tilde{\psi}\left(\bar{\phi}\right) \xrightarrow{\mathcal{R}^*} \psi_m \xrightarrow{\mathcal{I}} \psi_{f,m}$ and (2) $\tilde{\psi}\left(\bar{\phi}\right) \xrightarrow{\mathcal{I}} \tilde{\psi}_f \xrightarrow{\mathcal{R}^*} \psi_{f,m}$. Higher accuracy is attained by computing gas-phase quantities at the (fixed) grid points rather than at the (moving) drop locations, hence we adopt procedure (1), in which the unfiltered variable models computed at the grid points are denoted as ψ_m.

The ψ_m that we consider are those for which Okong'o & Bellan (2000) conducted an *a priori* study, which however did not examine the filtered source terms resulting from these ψ_m. All the models of Okong'o & Bellan (2000) are based on the filtered flow field $\tilde{\psi}$, and some models also use the SGS standard deviation, σ_{SGS}, where $\sigma^2_{SGS}\left(\tilde{\psi}\right) = \widetilde{\psi^2} - \tilde{\psi}^2$ (see (5.1) and (5.2)). We will compare four ψ_m, denoted as:

(a) Ideal, which precisely replicates ψ, i.e. $\psi_m = \psi$. Although such a model cannot be constructed in LES, in the *a priori* analysis it allows us to assess the best-case scenario when errors due to modeling the unfiltered flow field are eliminated.

(b) Baseline, which uses the filtered field, i.e. $\psi_m = \tilde{\psi}$. This model neglects SGS effects on drop evolution.

(c) Random, which uses a random function for ψ_m, specifically, a Gaussian with mean $\tilde{\psi}$ and standard deviation σ_{SGS}. This model is based on the *a priori* analysis of Okong'o & Bellan (2000), which showed this distribution to be applicable to the gas-phase variables within the filtering volumes.

(d) Deterministic, which uses an analytically derived model of Okong'o & Bellan (2000)

wherein

$$\psi_m = \tilde{\psi} - \overline{\sigma} sign\left(\nabla^2 \tilde{\psi}\right), \tag{4.1}$$

with the filtered standard deviation $\overline{\sigma} = \sqrt{\overline{\sigma^2}}$ modeled as

$$\overline{\sigma^2} = \left(\sqrt{\widetilde{\psi\psi}} - \sqrt{\tilde{\psi}\tilde{\psi}}\right)^2 = \left(\sqrt{\sigma_{SGS}^2 + \tilde{\psi}\tilde{\psi}} - \sqrt{\tilde{\psi}\tilde{\psi}}\right)^2. \tag{4.2}$$

In LES, both σ_{SGS} and some components of $\tilde{\psi}$ (specifically, $\tilde{T}$ and $\tilde{p}$; see Okong'o & Bellan (2002)) must be modeled; however, for purposes of the present *a priori* analysis, we will use the actual $\tilde{\psi}$ and σ_{SGS} as calculated from the DNS database in order to decouple the assessment of the reconstruction process from the issue of modeling $\tilde{\psi}$ and σ_{SGS}. The modeling of σ_{SGS} is discussed in § 5.

The analysis here consists of using ψ_m to compute the drop far-field primitive variables ($\psi_{f,m}$), the source term contribution of individual drops ($S_{d,m} = S_d(\psi_{f,m}, Z)$) and the filtered source terms ($\bar{S}_m = \bar{S}(\psi_{f,m}, Z)$). For brevity, $\psi_{f,m}$, $S_{d,m}$ and $\bar{S}_m$ will be designated according to ψ_m as ideal, baseline, random or deterministic models. The results from the models will be compared to the 'exact' (i.e. DNS flow field) quantities (ψ_f, S_d and $\bar{S}$). Note that, because we are still considering the actual drop field, the ideal model here leads to the exact ψ_f, S_d and $\bar{S}$; therefore only the other three models will be assessed. We use the same method as in the DNS to interpolate the gas phase variables to the drop locations and to calculate S_d. Both $\bar{S}_m$ and $\bar{S}$ are calculated through (3.8), that is, at this juncture the exclusive difference them is in the use of ψ_m instead of ψ.

Comparisons of two quantities defined at all grid points, $\mathcal{X}(x_1, x_2, x_3)$ and $\mathcal{Y}(x_1, x_2, x_3)$, are performed using a least-squares (LS) fit of $\mathcal{Y} = b\mathcal{X}$ which leads to the slope

$$b = \frac{\langle\langle \mathcal{X}\mathcal{Y} \rangle\rangle}{\langle\langle \mathcal{X}\mathcal{X} \rangle\rangle} \tag{4.3}$$

and the correlation

$$\mathcal{R}(\mathcal{X},\mathcal{Y}) = \frac{\langle\langle\mathcal{X}\mathcal{Y}\rangle\rangle - \langle\langle\mathcal{X}\rangle\rangle\langle\langle\mathcal{Y}\rangle\rangle}{\sqrt{\left(\langle\langle\mathcal{X}^2\rangle\rangle - \langle\langle\mathcal{X}\rangle\rangle^2\right)}\sqrt{\left(\langle\langle\mathcal{Y}^2\rangle\rangle - \langle\langle\mathcal{Y}\rangle\rangle^2\right)}} \tag{4.4}$$

where $\langle\langle\rangle\rangle$ denotes averaging over all grid points. (For drop-based quantities, the averaging is performed over the ensemble of all relevant drops.) The analysis is here performed for TP600a2 at the transitional state and is based on the filtered flow fields obtained at two different filter widths, $\bar{\Delta} = 4\Delta x$ and $\bar{\Delta} = 8\Delta x$, where $\Delta x = \max(\Delta x_1, \Delta x_2, \Delta x_3)$ is the grid spacing with $\Delta x_1 \simeq \Delta x_2 \simeq \Delta x_3$ for our DNS database (see Table 1). Slopes b according to (4.3), where $\mathcal{Y}$ is the exact quantity and $\mathcal{X}$ is the model, are tabulated in Table 2 (for ψ_f), Table 3 (for S_d) and Table 4 (for $\bar{S}$).

Displayed in Table 2 is the assessment of the baseline, random and deterministic ψ_m in their prediction of ψ_f. For all models, the largest discrepancy is in the modeling of $u_{3,f}$, with errors (measured according to the deviation from the optimum slope of unity) of 8%, 11% and 6% for the baseline, random and deterministic ψ_m respectively when $\bar{\Delta} = 4\Delta x$. When $\bar{\Delta} = 8\Delta x$, the corresponding errors are 17%, 29% and 9%. Therefore, the deterministic $\psi_{f,m}$ is slightly better than the baseline $\psi_{f,m}$, while the random $\psi_{f,m}$ is slightly worse. Next, ψ_f and the three $\psi_{f,m}$ are used in (2.24) to calculate drop source terms (S_d or $S_{d,m}$); the slopes comparing S_d to the model predictions are listed in Table 3. The largest discrepancy is in the modeling of $S_{II,3,d}$, with errors of 21%, 71% and 28% for the baseline, random and deterministic models, respectively, for $\bar{\Delta} = 4\Delta x$, and as much as 61%, 89% and 69% for $\bar{\Delta} = 8\Delta x$. The behavior mimics that of Table 2, where $u_{3,f}$ was the least accurately modeled component of ψ_f. However, the modeling errors are much larger in $S_{d,m}$ than in $\psi_{f,m}$, especially for the random model which performs quite poorly, while now it is the baseline model rather than the deterministic model that performs best. All the slopes are less than unity, meaning that the source

terms will on average be over-predicted. Finally, the filtered source terms ($\bar{S}$), which are the quantities entering the LES equations, are shown in Table 4; these are computed by summing the (exact or modeled) drop source terms of Table 3 over all drops within each filtering volume. Similar to Table 3, the largest discrepancy is in the modeling of $\bar{S}_{II,3}$, with errors of 19%, 26% and 21% for the baseline, random and deterministic models, respectively, when $\bar{\Delta} = 4\Delta x$, and as much as 52%, 55% and 57% for $\bar{\Delta} = 8\Delta x$. The smallest discrepancy is in the modeling of $\bar{S}_I$ and is close to that in modeling $\bar{S}_{III}$. In comparing the results for $S_{d,m}$ and $\bar{S}_m$ we note that for $\bar{S}$ all the slopes for the random model tend to increase with respect to those of S_d (except for $\bar{S}_I$), whereas for the other two models, only the slopes of some momentum source terms ($S_{II,2}$ and $S_{II,3}$) consistently tend to increase. The baseline model is still the best, followed by the deterministic model, but the random model is now comparable to the other two. Similar to what was seen for S_d, for $\bar{S}$ all the slopes are less than unity, meaning that $\bar{S}$ will on average be over-predicted. Notably, the slopes for $\bar{S}$ listed in Table 4 are considerably lower those for ψ_f listed in Table 2, and all the models show definite deterioration with increased $\bar{\Delta}$.

This analysis indicates that with exact σ_{SGS}, the baseline model is generally no worse, and usually better than the more sophisticated random and deterministic models. This can partly be attributed to the non-linear nature of the relationship between ψ_f and S_d, since small discrepancies in $\psi_{f,m}$ seem to lead to much larger discrepancies in $S_{d,m}$. The errors in $\bar{S}_m$ are considerably larger than those in $\psi_{f,m}$. Furthermore, the magnitude of the error in $\psi_{f,m}$ shows no predictive ability for the error in the resulting $\bar{S}_m$. Apparently, the filter width is the main determinant regarding the accuracy of $\bar{S}_m$, since the errors consistently and dramatically increase with $\bar{\Delta}$. This analysis also suggests that, for reasonable models for σ_{SGS}, the effect on $\bar{S}_m$ of replacing the exact σ_{SGS} (available here

from DNS but not available in typical LES) with a modeled σ_{SGS} will not be significant, since the baseline model is equivalent to the random or deterministic models with σ_{SGS} set to zero.

4.2. *Computational-drop modeling*

Having studied the effect of the unfiltered-variable modeling on the source terms, we now turn to the issue of reducing the number of computed drops. In the simple formulation considered here, each computational drop represents a fixed number of actual drops. That is, if the number of real drops is N_α and the number of computational drops is N_β, then each computational drop β represents N_R drops, where $N_R = N_\alpha/N_\beta$ is the ratio between the number of actual drops and the number of computational drops. The filtered source terms are then computed for the N_β drops, and scaled by N_R leading to

$$\bar{S}_m\left(\psi_{f,m}\left(\bar{\phi}\right), \bar{Z}\right) = N_R \sum_\beta \frac{1}{V_f}\left[S_d\left(\psi_{f,m}\left(\bar{\phi}\right), \bar{Z}\left(N_R\right)\right)\right]_\beta . \tag{4.5}$$

As in (3.8), the summation is over the drops within the filtering volume V_f, but now over a representative drop field ($\bar{Z}$) rather than the actual drops (Z). The source term contributions for each computational drop are computed in the same manner as for actual drops, that is, the representative nature of each drop is entirely embodied in the parameter N_R. The unfiltered variables (ψ_f) required for calculating each drop's source term contributions are modeled ($\psi_{f,m}$), as described in § 4.1. The filtered source term models ($\bar{S}_m$) will be designated according to the underlying primitive variable model (ψ_m) as ideal, baseline, random or deterministic. The modeled filtered source terms are next compared to the exact (i.e. DNS) filtered source terms $\bar{S}\left(\psi_f, Z\right)$. Note that the ideal model leads to the exact $\bar{S}$ only on the actual drop field ($N_R = 1$). For the analysis undertaken here, the computational drops are selected from the DNS drops by extracting them from the array containing Z with a stride of N_R; each computational drop retains

the characteristics (mass, location, velocity, temperature) of a physical drop. In LES, no such correspondence between computational and physical drops would exist, because the unfiltered flow field that governs the evolution of physical drops would not be available. Thus, in a LES the choice of N_R would be based on experimental data in conjunction with results from the present analysis.

To illustrate the effect of increasing N_R (decreasing the number of computational drops), in Figure 2 are the (x_1, x_3) homogeneous-plane averages and RMS of $\bar{S}_I$ and its models. The results for $\bar{S}_m$ are labeled according to the ψ_m used (ideal, baseline, random, deterministic), while those for $\bar{S}$ are labeled as exact. These plots for $N_R = 1, 8$ and 64 are not intended to be typical, but rather to visualize the global comparisons to be presented below. Clearly, in the middle of the layer there is strong evaporation, as indicated by the average $\bar{S}_I$ being positive. In the lower stream, on average $\bar{S}_I$ is negative, indicating net condensation; further scrutiny revealed that at some locations there is also evaporation occurring. As shown by the small RMS in the lower stream, the magnitude of condensation/evaporation is small. Returning to the issue of computational-drop modeling, Figure 2 shows that $\bar{S}_I$ is generally overpredicted by the models. Whereas on average, the models do not seem to show much dependence on N_R, the RMS shows a clear deterioration with N_R. The greatest error in $\bar{S}_{I,m}$ occurs in the middle of the layer where the strongest evaporation occurs and where the filtered flow field differs most from the unfiltered flow field. In contrast, near the boundaries the filtered flow field is almost identical to the unfiltered one. Since the models are relatively more accurate at the lower stream boundary, where the non-zero $\bar{S}_I$ shows that the drops are still evaporating/condensing, the indications are that drop evaporation is not by itself the cause of errors in the filtered source term models. Rather, errors arise from the imprecision in representing the actual drop field by the computational drop field, since the ideal model

(which uses the actual unfiltered variables) gives the same results as the other models near the lower boundary. Given that the errors due to modeling the unfiltered flow field (see § 4.1) are unavoidable in LES, we want to determine the conditions under which the additional errors introduced by the computational-drop modeling are acceptably small.

To quantify the effect of increasing N_R, slopes equivalent to those in Table 4 are plotted in figures 3 and 4 for $\bar{S}_I$ (figures 3*a* and 3*b*), $\bar{S}_{III}$ (figures 3*c* and 3*d*) $\bar{S}_{II,1}$ (figures 4*a* and 4*b*) $\bar{S}_{II,2}$ (figures 4*c* and 4*d*) $\bar{S}_{II,3}$ (figures 4*e* and 4*f*) for $\bar{\Delta}$ of $4\Delta x$ and $8\Delta x$, respectively. These figures are for $N_R = 1, 2, 4, 8, 16, 32, 64$ for all filtered source term models; all quantities are compared to $\bar{S}$. (Note: The slopes for $N_R = 1$ were previously presented in Table 4.) In figures 3 and 4, all the slopes are smaller than unity, meaning that all the models overestimate the source terms. Generally, the baseline and deterministic models are quite similar, and better than the random model. Consistently, the ideal model gives the best prediction for $\bar{S}$; its relative superiority is significant at the larger filter width, and at the smaller filter width when N_R is small. For the smaller filter width at larger N_R, all the models give similar predictions. The accuracy of the models declines with N_R, but not at the same rate for all source terms as $\bar{S}_{III}$ seems to be best predicted whereas $\bar{S}_{II,3}$ seems to be the worst predicted with the strongest error growth with N_R.

From figures 3 and 4, it can be concluded that for small N_R (more computational drops) the inaccuracies in $\psi_{f,m}$ are a much stronger source of error than is the effect of computational-drop modeling ($N_R > 1$). This explains why, when using ψ_f, the ideal model $\bar{S}_m$ improves for fixed N_R as $\bar{\Delta}$ is increased from $4\Delta x$ to $8\Delta x$ since the filtering volume is increased and the number of drops within each filtering volume is accordingly increased, giving a better accuracy; whereas the opposite is observed with all the other $\bar{S}_m$ because as $\bar{\Delta}$ increases, information is lost during the gas-phase variable modeling, resulting in decreasing accuracy (as $\bar{\Delta}$ increases, $\tilde{\psi}$ is more unlike ψ, see Table 2). How-

ever, for large N_R (fewer computational drops), larger than about 8, the effect of having few drops dominates, as can be seen by the increasing convergence of the slopes from the ideal $\bar{S}_m$ to those from the other $\bar{S}_m$ for larger N_R. Figures 3 and 4 also show the effect of the nonlinear relationship between $\psi_{f,m}$ and $\bar{S}_m$ in that a proportional reduction in grid resolution and number of drops does not give the same error in the filtered source terms. That is, increasing $\bar{\Delta}$ from $4\Delta x$ to $8\Delta x$ means an eight-fold increase in the filtering volume, but an eight-fold decrease in the number of drops ($N_R = 1, 2, 4, 8$ compared to $N_R = 8, 16, 32, 64$, respectively) does not give the same error in $\bar{S}_m$. For example, an eight-fold increase in filtering volume leads to a doubling of the error on $\bar{S}_{III}$ for $N_R = 1$, but an eight-fold decrease in the number of drops leads to errors on $\bar{S}_{III}$ that are either much larger or much smaller, without consistent trend as a function of N_R. In LES the effect of modeling ψ_f is unavoidable and most likely $\bar{\Delta}$ would have been selected according to the gas-phase resolution requirements; but apparently N_R should be considered as a parameter to be optimized along with $\bar{\Delta}$.

The above results concerning the computational drops were obtained at a transitional state. It is pertinent to inquire whether the overprediction of the filtered source terms is unique to this time station, or rather a general occurrence. To this end, the analysis of $\bar{S}_m$ was repeated at t^*=20, 45 and 80, corresponding to time stations before the first pairing, between the first and second pairings and at the end of the second pairing. The results are plotted in along with those at t^*=105, in terms of the maximal percentage error (greatest deviation from unity over the five source terms, multiplied by 100) in figure 5 for t^*=20 (figures 5*a* and 5*b*), t^*=45 (figures 5*c* and 5*d*), t^*=80 (figures 5*e* and 5*f*), t^*=105 (figures 5*g* and 5*h*) at $\bar{\Delta}$ of $4\Delta x$ and $8\Delta x$. Figures 5*g* and 5*h* represent the data in figures 3 and 4 (at t^*=105), and the remarks made when discussing those figures are even more evident: (1) the effect of modeling ψ_f is dominant at the larger $\bar{\Delta}$, where the error is initially

large but not so sensitive to N_R, (2) the effect of modeling ψ_f is significant at the smaller $\bar{\Delta}$ for smaller N_R but not at larger N_R, (3) the baseline model performs best, followed closely by the deterministic model, with the random model giving the worst predictions, and (4) decreasing the number of drops proportionally to the increase in filtering volume size does not necessarily maintain the filtering error. In considering the pre-transitional time stations, the trends at a given N_R seem to be as follows: (1) for the smaller $\bar{\Delta}$, the error seems insensitive to time, except for the lowest $N_R = 1$ or 2 where the error clearly grows with time, and (2) for the larger $\bar{\Delta}$, the error generally grows with time, with more pronounced error growth at smaller values of N_R.

From this *a priori* study, the indications are that the unfiltered flow field models perform better for smaller filter widths; however, only at small values of N_R (below about 8 for $\bar{\Delta} = 4\Delta x$) does this translate into improved accuracy of filtered source term models. On the other hand, for larger filter widths, there is little to be gained by using small N_R, since the error growth with N_R is modest; however, the filtered source term models will be less accurate than at the smaller filter width. None of the models considered yields particularly good predictions for the filtered source terms, with errors ranging from 20% to 90%. However, this does not necessarily preclude their use in LES, since from the budgets of the LES equations (Okong'o & Bellan (2002)), the filtered source terms are an order of magnitude smaller than the largest terms. The sensitivity of flow field and drop evolution to filtered source term errors can only be determined by performing an *a posteriori* LES study.

5. Subgrid Scale models

This portion of the *a priori* study is devoted to analyzing models for the SGS fluxes (defined in (3.6)) appearing in the LES equations (3.3)–(3.5). This activity involves the

consideration of several possible functional forms for the fluxes, which contain coefficients of proportionality to be determined through calibration on the DNS transitional flow field. Additionally, some of the filtered source term models described in § 4.1 use the SGS variance σ_{SGS}, here defined as

$$\sigma^2_{SGS}(\tilde{u}_1) = \widetilde{u_1 u_1} - \tilde{u}_1\tilde{u}_1,\ \sigma^2_{SGS}(\tilde{u}_2) = \widetilde{u_2 u_2} - \tilde{u}_2\tilde{u}_2,\ \sigma^2_{SGS}(\tilde{u}_3) = \widetilde{u_3 u_3} - \tilde{u}_3\tilde{u}_3, \quad (5.1)$$

$$\sigma^2_{SGS}\left(\tilde{T}\right) = \widetilde{T^2} - \left(\tilde{T}\right)^2, \quad \sigma^2_{SGS}\left(\tilde{Y}_V\right) = \widetilde{Y_V Y_V} - \tilde{Y}_V\tilde{Y}_V, \quad \sigma^2_{SGS}(\bar{p}) = \overline{p^2} - (\bar{p})^2. \quad (5.2)$$

The SGS variances have a similar form to the SGS fluxes (in fact, $\sigma^2_{SGS}(\tilde{u}_1) = \tau_{11}$, $\sigma^2_{SGS}(\tilde{u}_2) = \tau_{22}$ and $\sigma^2_{SGS}(\tilde{u}_3) = \tau_{33}$) and we propose to model them in the same way.

5.1. *Functional forms*

We consider here the following three typical SGS models:

(*a*) The Smagorinsky (SM) model for the SGS fluxes is

$$\tau_{ij} - \frac{1}{3}\tau_{kk}\delta_{ij} = -C_{SM}\bar{\Delta}^2 S(\bar{\phi})\left[S_{ij}(\bar{\phi}) - \frac{1}{3}S_{kk}(\bar{\phi})\delta_{ij}\right],$$

$$\eta_j = -C_{SM}\bar{\Delta}^2 S(\bar{\phi})\frac{1}{2}\frac{\partial\tilde{Y}_V}{\partial x_j}, \quad \zeta_j = -C_{SM}\bar{\Delta}^2 S(\bar{\phi})\frac{1}{2}\frac{\partial\tilde{h}}{\partial x_j}, \quad (5.3)$$

where

$$S^2(\phi) = S_{ij}(\phi)S_{ij}(\phi). \quad (5.4)$$

To model τ_{kk}, which may be important for compressible turbulence, we use the Yoshizawa (1986) (YO) model

$$\tau_{kk} = C_{YO}\bar{\Delta}^2 S^2(\bar{\phi}). \quad (5.5)$$

The SM model is based on eddy-viscosity considerations which cannot be directly extended to model the σ^2_{SGS} of $\tilde{T}$, $\tilde{Y}_V$ and $\bar{p}$.

(*b*) The Gradient (GR) model for the SGS fluxes is

$$\tau_{ij} = C_{GR}\bar{\Delta}^2\frac{\partial\tilde{u}_i}{\partial x_k}\frac{\partial\tilde{u}_j}{\partial x_k}, \quad \eta_j = C_{GR}\bar{\Delta}^2\frac{\partial\tilde{Y}_V}{\partial x_k}\frac{\partial\tilde{u}_j}{\partial x_k}, \quad \zeta_j = C_{GR}\bar{\Delta}^2\frac{\partial\tilde{h}}{\partial x_k}\frac{\partial\tilde{u}_j}{\partial x_k}, \quad (5.6)$$

while the GR model for $\sigma^2_{SGS}\left(\tilde{\psi}\right)$ is

$$\sigma^2_{SGS}\left(\tilde{\psi}\right) = C_{GR}\bar{\Delta}^2 \frac{\partial\tilde{\psi}}{\partial x_k}\frac{\partial\tilde{\psi}}{\partial x_k}. \tag{5.7}$$

Theoretically (i.e. from a Taylor series expansion, see Appendix A) $C_{GR} = 1/12$ for a cubic top-hat filter.

(c) The Scale-Similarity (SS) model for the SGS fluxes is

$$\tau_{ij} = C_{SS}\left(\widehat{\tilde{u}_i\tilde{u}_j} - \hat{\tilde{u}}_i\hat{\tilde{u}}_j\right), \quad \eta_j = C_{SS}\left(\widehat{\tilde{Y}_V\tilde{u}_j} - \hat{\tilde{Y}}_V\hat{\tilde{u}}_j\right), \quad \zeta_j = C_{SS}\left(\widehat{\tilde{h}\tilde{u}_j} - \hat{\tilde{h}}\hat{\tilde{u}}_j\right), \tag{5.8}$$

and the SS model for $\sigma_{SGS}\left(\tilde{\psi}\right)$ is

$$\sigma^2_{SGS}\left(\tilde{\psi}\right) = C_{SS}\left[\widehat{\left(\tilde{\psi}\right)^2} - \left(\hat{\tilde{\psi}}\right)^2\right], \tag{5.9}$$

where the overhat $\hat{()}$ denotes (unweighted) filtering at the test-filter level $\hat{\Delta} \geqslant \bar{\Delta}$. Scale-similarity implies that $C_{SS} = 1$ for identical grid and test filters (Bardina *et al.* (1980), Pruett & Adams (2000)), however, practically its true value depends on the situation under study as well as on the filter type and on the ratio $\hat{\Delta}/\bar{\Delta}$ (see Appendix B). For example, Liu *et al.* (1994) found from analysis of experimental data that for turbulent jets $0.3 \leqslant C_{SS} \leqslant 0.6$, whereas the rigorous derivation of Pruett *et al.* (2001) led to $C_{SS} = a_2/c_2$ for second-order grid and test filters whose second-order coefficients in the Taylor expansions are a_2 and c_2, respectively.

Although generally each SGS quantity may have a model coefficient value different from the others and furthermore, the coefficient may be spatially and temporally varying, for simplicity, in this study, all SGS quantities will use the same value of the model coefficient (C_{SM}, C_{GR} or C_{SS}) which is taken spatially and temporally constant. In keeping with the LES philosophy of reduced computational effort, more complicated model coefficients are usually considered only after constant coefficients prove inadequate *a posteriori*.

5.2. *Constant-coefficient calibration*

The availability of a DNS database allows *a priori* calibration of the constant coefficient appearing in each of the SGS flux models under consideration. (The coefficient may also be calibrated *a posteriori* by performing LES and attempting to match the filtered DNS results.) The calibration procedure used here consists of three stages:

(a) Calculation of the coefficient for each SGS quantity: To this end, we use LS fits of the SGS quantities to their models to compute the slope, b, which would be the constant coefficient, and the correlation, $\mathcal{R}$, according to (4.3) and (4.4). If $\mathcal{X}$ is the model (without the coefficient) and $\mathcal{Y}$ is the SGS quantity, then the slope is the constant coefficient. $\mathcal{R}^2$ measures the fraction of the variation in $\mathcal{Y}$ that is due to the variation in $\mathcal{X}$ (Ayyub & McCuen (1997)); therefore $\mathcal{R}$ is an indicator of the suitability of using a constant coefficient and ideally would be unity.

(b) Calculation of the coefficient for all SGS quantities: To obtain a single coefficient, we average the slopes for the individual SGS quantities. The standard deviation of these slopes measures their variation from the average. Therefore, the smaller the standard deviation relative to the average slope, the more suitable is the average slope for being the single coefficient for all the SGS quantities.

(c) Calculation of the coefficient for the SGS model: To obtain a single coefficient, we calculate the average slopes on many filtered flow fields (or realizations of the same flow), and develop the best value for the SGS model coefficient. This coefficient may be found to depend on filter width, Re_0, $M_{c,0}$ flow configuration, etc. The applicability of the coefficient will generally be limited to the types of flow for which it was calibrated, which constitutes the main drawback of the constant-coefficient method. However, the hope of the constant-coefficient LES methodology is that the SGS are somewhat insensitive to the large scale flow, and that their calibration on a geometrically simple transitional

flow will be applicable to a variety of other flows. In this study, the focus is on possible dependence of SGS models on the presence or absence of drops, and on the filter width. This dependence of the coefficient on the flow field is measured by performing t-tests of statistical significance on the average slopes obtained in the second stage described above.

The calibration procedure outlined above is performed for the SM, YO, GR and SS models. For the SS model, two test-filter widths ($\hat{\Delta} = \bar{\Delta}$ and $\hat{\Delta} = 2\bar{\Delta}$) are investigated. The analysis is performed for the SP600 and TP600a2 databases at the transitional states (t^*=100 and t^*=105 respectively) at two different filter widths ($\bar{\Delta} = 4\Delta x$ and $\bar{\Delta} = 8\Delta x$) for a total of 4 data sets. These two cases are selected for analysis because they have the higher Re_0 (see Table 1). The SGS quantities analyzed are $\{\bar{\rho}\tau_{ij},\ \bar{\rho}\zeta_j,\ \sigma^2_{SGS}\left(\tilde{T}\right),\ \sigma^2_{SGS}(\bar{p})\}$ (11 quantities) for case SP600 (for which $\tilde{Y}_V = 0$, $\eta_j = 0$) and $\{\bar{\rho}\tau_{ij},\ \bar{\rho}\zeta_j,\ \bar{\rho}\eta_j,\ \sigma^2_{SGS}\left(\tilde{T}\right),\ \sigma^2_{SGS}\left(\tilde{Y}_V\right),\ \sigma^2_{SGS}(\bar{p})\}$ (15 quantities) for case TP600a2. The $\sigma^2_{SGS}(\tilde{u}_i)$ are excluded because $\sigma^2_{SGS}(\tilde{u}_i) = \tau_{ij}$ for $i = j$ and are therefore already represented in the set of compared quantities. For each model, the slopes for each SGS quantity are presented in Tables 5–9, along with the average and the standard deviation of the slopes and the average of the correlations. We apply a two-tailed t-test for equality of means to these slopes (at a 5% level of significance, assuming unequal variances), and present the results of the t-tests in Tables 10–13. If the t-test indicates that the average slopes are equal, we take the mean of the average slopes (of the appropriate data sets) as the model coefficient. The analysis of the models, including the calibrated coefficients can be summarized as follows:

(a) Smagorinsky model (Table 5) and Yoshizawa model (Table 6): The correlation between the models and the SGS quantities is poor (0.24 to 0.31), and the large standard deviation is due to the large spread of the individual slopes. The t-test indicates that

the same coefficient can be applied to all four data sets; the mean value of the average slopes is 0.072. For τ_{kk}, the YO model (Table 6) has a correlation of about 0.8, which is considerably better than that for the SM model. From the four data sets considered, the mean value is $C_{YO} = 0.314$. This large value of C_{YO} compared to that of C_{SM} indicates that τ_{kk} should not be neglected, in contrast to the results of Erlebacher *et al.* (1992) for isotropic turbulence. However, since the Smagorinsky model generally correlates poorly with the SGS quantities, it is not clear whether any benefit would be derived from not neglecting τ_{kk}. (Neglecting τ_{kk} does not alter the average slope or the calibrated coefficient.) The calibration of the SM model along with the YO model leads to the coefficients

$$C_{SM} = 0.072, \; C_{YO} = 0.314. \tag{5.10}$$

The value obtained here of $C_{SM} = 0.072$ is higher than $C_{SM} = 0.17^2 \simeq 0.029$ used by Vreman *et al.* (1997), which was found to be too dissipative; the calibrated values will lead to a SM model that is even more dissipative.

(*b*) Gradient model (Table 7): The correlation between models and SGS quantities is excellent (0.91 to 0.97). From the t-test, the average slopes are equal for all four data sets, with a mean value across the four data sets of 0.152. The calibration leads to the GR model coefficient as

$$C_{GR} = 0.152. \tag{5.11}$$

(*c*) Similarity model (Tables 8 and 9): The correlation between models and SGS quantities ranges from good to excellent (0.72 to 0.94), with better correlation for $\hat{\Delta} = \bar{\Delta}$. From the t-test, the average slopes are statistically equal when comparing SP600 to TP600a2, but not when comparing $\bar{\Delta} = 4\Delta x$ to $\bar{\Delta} = 8\Delta x$. Therefore the SS model

calibration yields

$$C_{SS} = 1.606 \text{ for } \hat{\Delta} = \bar{\Delta},\ \bar{\Delta} = 4\Delta x, \tag{5.12}$$

$$C_{SS} = 1.996 \text{ for } \hat{\Delta} = \bar{\Delta},\ \bar{\Delta} = 8\Delta x, \tag{5.13}$$

$$C_{SS} = 0.642 \text{ for } \hat{\Delta} = 2\bar{\Delta},\ \bar{\Delta} = 4\Delta x, \tag{5.14}$$

$$C_{SS} = 0.808 \text{ for } \hat{\Delta} = 2\bar{\Delta},\ \bar{\Delta} = 8\Delta x. \tag{5.15}$$

Since the theoretical model coefficient is unity, the closest value to theory is attained with $\bar{\Delta} = 8\Delta x$ and $\hat{\Delta} = 2\bar{\Delta}$. The coefficients at $\hat{\Delta} = \bar{\Delta}$ are about 2.5 times larger than those at $\hat{\Delta} = 2\bar{\Delta}$ for the same $\bar{\Delta}$, so there is a strong coefficient dependence on $\hat{\Delta}/\bar{\Delta}$. On the other hand, the coefficients at $\bar{\Delta} = 4\Delta x$ are about 80% of those at $\bar{\Delta} = 8\Delta x$, so the coefficient dependence on $\bar{\Delta}/\Delta x$ is much weaker than that on $\hat{\Delta}/\bar{\Delta}$. It can be analytically shown that there should be a coefficient dependence on $\hat{\Delta}/\bar{\Delta}$ (Pruett *et al.* (2001); see Appendix B) such that C_{SS} decreases with increasing $\hat{\Delta}/\bar{\Delta}$. However, the coefficient dependence on $\bar{\Delta}/\Delta x$ being weak, suggests that the flow field is not quite scale-similar, perhaps due to the simulations being transitional rather than in the fully turbulent regime.

These results are consistent with the *a priori* investigation of Pruett & Adams (2000) for the decay of isotropic turbulence in which the SM model correlated poorly with the exact stresses and the SS model correlated remarkably well, particularly when the grid and test filter were identical. However, correlations for the GR model are here much better when compared to those obtained by Pruett & Adams (2000) (0.9 compared to 0.6); this may be due to their use of the same form of the GR model as has been analyzed here that applies only to cubic top-hat filters (see Appendix A), and which is inconsistent with their filter (one-parameter Pade-type filter). At this juncture, the prospects for successful TP LES using the SM model seem poor, since drop evolution in TP flows

is strongly dependent on the local conditions which are poorly captured by this model. The model calibration exercise also suggests that, to overcome deficiencies in the GR or SS model that have been found in some *a posteriori* studies (e.g.Vreman *et al.* (1997) who used the theoretical coefficients $C_{SS} = 1$, $C_{GR} = 1/12$), it may be more fruitful to adjust C_{GR} or C_{SS} rather than add the SM model (leading to 'mixed' models) and then attempt to adjust the SM coefficient.

The most encouraging result of this calibration is the suggestion that coefficients calibrated on compressible SP flow are statistically equivalent to those for TP flow with evaporating drops, implying that SGS models already developed for SP flows may be applied to the SGS fluxes in TP flows. However, since the *a priori* study does not include either the effect of the flow field evolution on the drops or the interaction among all scales inherent in turbulence, *a posteriori* studies are needed to bear out this implication.

6. Summary and conclusions

A priori LES analysis has been performed on a database obtained from Direct Numerical Simulation (DNS) of a three-dimensional temporal mixing layer with evaporating drops. The DNS database consists of transitional states attained by layers with different initial Reynolds numbers and initial liquid-phase mass loadings. For DNS, the gas-phase equations are written in an Eulerian frame for two perfect gas species (carrier gas and vapor emanating from the drops), while the liquid-phase equations are written in a Lagrangian frame, tracking each drop. The drops act as point sources of mass, momentum and energy into the gas phase, while the gas phase acts as the drop far-field to affect the mass, position and temperature of each drop. LES equations governing the evolution of a spatially filtered gas-phase flow field are derived by filtering the gas-phase DNS equations. Since these equations pertain to the large scales, the resolution can be decreased,

but when doing so the small scales need to be modeled. Consistently, compared to the physical drops in DNS, a reduced number of 'computational' drops should be tracked in LES.

The LES models evaluated on the DNS database are of two types: those for the filtered source terms representing the effect of the drops on the filtered flow field, and those for the subgrid scale (SGS) fluxes arising from filtering the convective terms in the gas-phase DNS equations. The unfiltered flow field is required for the calculation of drop-based quantities but would not be available in LES; therefore, various approximations were attempted for it, namely, the filtered flow field and the filtered flow field plus corrections based on the SGS variances. All of the filtered source term models were found to overestimate filtered source terms, with the relative error of modeling the unfiltered flow field compared to that of using computational drops showing a complex dependence on filter width and number of computational drops. Generally, the performance of the models deteriorates with decreasing number of computational drops.

To complete the LES modeling, constant-coefficient Smagorinsky, Gradient and Scale-Similarity models for the SGS fluxes were assessed and calibrated on the DNS database. The Gradient and Scale-Similarity models showed excellent correlation with the SGS quantities, while the Smagorinsky model performed poorly. Calibrated values of the SGS model coefficients were computed for various filtered flow fields; the values were compared for transitional states generated from single-phase (SP) and two-phase (TP) DNS which had the same initial Reynolds number and grid size and resolution. For all SGS flux models, these coefficients were statistically equivalent when computed on SP or TP flows. Additionally, for the Smagorinsky and Gradient model, these coefficients were statistically insensitive to the filter width, whereas for the Scale-Similarity model, the coefficients depended on the filter widths used.

Although some of the models presented seem promising, the true test of their appropriateness will be in *a posteriori* studies. Such studies are needed to determine whether these models will lead to the proper evolution of the filtered flow field and of the computational drops, and to appropriate interaction between the resolved and modeled (SGS) flow field. Of particular interest will be the behavior of the models for the filtered source terms as the number of computational drops is decreased.

Appendix A. Derivation of gradient model

The gradient model (Clark *et al.* (1979)) can be derived starting from the Taylor series expansion for a variable ψ_i,

$$\psi_i(\mathbf{x}) = \psi_i(\mathbf{x}_0) + \frac{\partial \psi_i}{\partial x_k}(\mathbf{x}_0)(x_k - x_{k_0}) + \frac{\partial^2 \psi_i}{\partial x_k \partial x_l}(\mathbf{x}_0)\tfrac{1}{2}(x_k - x_{k_0})(x_l - x_{l_0}) + O(\bar{\Delta}^3). \tag{A 1}$$

Filtering this expansion leads to

$$\bar{\psi}_i = \psi_i(\mathbf{x}_0) + \frac{\partial \psi_i}{\partial x_k}(\mathbf{x}_0)\overline{(x_k - x_{k_0})} + \frac{\partial^2 \psi_i}{\partial x_k \partial x_l}(\mathbf{x}_0)\tfrac{1}{2}\overline{(x_k - x_{k_0})(x_l - x_{l_0})} + O(\bar{\Delta}^3). \tag{A 2}$$

Multiplying the series expansions for the variables ψ_i and ψ_j, then filtering yields

$$\begin{aligned}\overline{\psi_i\psi_j} = {} & \psi_i(\mathbf{x}_0)\psi_j(\mathbf{x}_0) + \left[\psi_i(\mathbf{x}_0)\frac{\partial \psi_j}{\partial x_k}(\mathbf{x}_0) + \psi_j(\mathbf{x}_0)\frac{\partial \psi_i}{\partial x_k}(\mathbf{x}_0)\right]\overline{(x_k - x_{k_0})} \\ & + \left[\psi_i(\mathbf{x}_0)\frac{\partial^2 \psi_j}{\partial x_k \partial x_l}(\mathbf{x}_0) + \psi_j(\mathbf{x}_0)\frac{\partial^2 \psi_i}{\partial x_k \partial x_l}(\mathbf{x}_0)\right]\tfrac{1}{2}\overline{(x_k - x_{k_0})(x_l - x_{l_0})} \\ & + \frac{\partial \psi_i}{\partial x_k}(\mathbf{x}_0)\frac{\partial \psi_j}{\partial x_l}(\mathbf{x}_0)\overline{(x_k - x_{k_0})(x_l - x_{l_0})} + O(\bar{\Delta}^3).\end{aligned} \tag{A 3}$$

Multiplying the series expansions for the variables $\bar{\psi}_i$ and $\bar{\psi}_j$ yields

$$\begin{aligned}\bar{\psi}_i\bar{\psi}_j = {} & \psi_i(\mathbf{x}_0)\psi_j(\mathbf{x}_0) + \left[\psi_i(\mathbf{x}_0)\frac{\partial \psi_j}{\partial x_k}(\mathbf{x}_0) + \psi_j(\mathbf{x}_0)\frac{\partial \psi_i}{\partial x_k}(\mathbf{x}_0)\right]\overline{(x_k - x_{k_0})} \\ & + \left[\psi_i(\mathbf{x}_0)\frac{\partial^2 \psi_j}{\partial x_k \partial x_l}(\mathbf{x}_0) + \psi_j(\mathbf{x}_0)\frac{\partial^2 \psi_i}{\partial x_k \partial x_l}(\mathbf{x}_0)\right]\tfrac{1}{2}\overline{(x_k - x_{k_0})(x_l - x_{l_0})} \\ & + \frac{\partial \psi_i}{\partial x_k}(\mathbf{x}_0)\frac{\partial \psi_j}{\partial x_l}(\mathbf{x}_0)\overline{(x_k - x_{k_0})}\,\overline{(x_l - x_{l_0})} + O(\bar{\Delta}^3).\end{aligned} \tag{A 4}$$

Then, the general form of the gradient model, valid for any filter, is

$$\overline{\psi_i\psi_j} - \bar{\psi}_i\bar{\psi}_j = \frac{\partial\psi_i}{\partial x_k}\frac{\partial\psi_j}{\partial x_l}\left[\overline{(x_k - x_{k_0})(x_l - x_{l_0})} - \overline{(x_k - x_{k_0})}\,\overline{(x_l - x_{l_0})}\right]. \tag{A 5}$$

Now, for a top hat filter

$$\overline{\psi}(\mathbf{x}_0) = \frac{1}{V_f}\int_{V_f}\psi(\mathbf{x})\,dV \tag{A 6}$$

where V_f is the filtering volume. Then, if $\mathbf{x}_0$ is the centroid of the filtering volume,

$$\overline{(x_k - x_{k_0})} = \frac{1}{V_f}\int_{V_f}(x_k - x_{k_0})\,dV = 0. \tag{A 7}$$

The terms $\overline{(x_k - x_{k_0})(x_l - x_{l_0})}$ are the moments of inertia, which in the case of a cubic top-hat filter with symmetrical filtering volumes are $\frac{1}{12}\bar{\Delta}^2\delta_{kl}$ leading to

$$\overline{\psi_i\psi_j} - \bar{\psi}_i\bar{\psi}_j = \frac{1}{12}\bar{\Delta}^2\frac{\partial\psi_i}{\partial x_k}\frac{\partial\psi_j}{\partial x_k} \tag{A 8}$$

Approximating the ψ_i derivatives by $\bar{\psi}_i$ derivatives leads to the gradient model for a cubic top-hat filter as

$$\overline{\psi_i\psi_j} - \bar{\psi}_i\bar{\psi}_j = C_{GR}\bar{\Delta}^2\frac{\partial\bar{\psi}_i}{\partial x_k}\frac{\partial\bar{\psi}_j}{\partial x_k}. \tag{A 9}$$

This model is applied to the Favre-filtered quantities as

$$\widetilde{\psi_i\psi_j} - \tilde{\psi}_i\tilde{\psi}_j = C_{GR}\bar{\Delta}^2\frac{\partial\tilde{\psi}_i}{\partial x_k}\frac{\partial\tilde{\psi}_j}{\partial x_k}. \tag{A 10}$$

This expression can be derived from (A 5) by replacing the unweighted filtering with Favre-filtering, namely

$$\widetilde{\psi_i\psi_j} - \tilde{\psi}_i\tilde{\psi}_j = \frac{\partial\psi_i}{\partial x_k}\frac{\partial\psi_j}{\partial x_l}\left[\widetilde{(x_k - x_{k_0})(x_l - x_{l_0})} - \widetilde{(x_k - x_{k_0})}\widetilde{(x_l - x_{l_0})}\right] + O\left(\bar{\Delta}^3\right) \tag{A 11}$$

then using $\widetilde{(x_k - x_{k_0})} \simeq \overline{(x_k - x_{k_0})}$ and $\widetilde{(x_k - x_{k_0})(x_l - x_{l_0})} \simeq \overline{(x_k - x_{k_0})(x_l - x_{l_0})}$ and approximating the ψ_i derivatives by $\tilde{\psi}_i$ derivatives.

The model coefficient C_{GR} can be expected to larger than its theoretical value, because, since $\bar{\psi}_i$ is smoother than ψ_i, $\partial\bar{\psi}_i/\partial x_k$ will have smaller magnitude than $\partial\psi_i/\partial x_k$.

Appendix B. Test-filter ratio dependence of scale-similarity model

The scale similarity model is (Bardina *et al.* (1980))

$$\overline{\psi_i\psi_j} - \bar{\psi}_i\bar{\psi}_j = C_{SS}\left(\widehat{\bar{\psi}_i\bar{\psi}_j} - \hat{\bar{\psi}}_i\hat{\bar{\psi}}_j\right), \tag{B 1}$$

where the overhat $\hat{()}$ denotes filtering at the test-filter width $\hat{\Delta} \geqslant \bar{\Delta}$. For clarity, the derivation that follows uses the unweighted filter. The application to Favre-filtered quantities is through replacing the unweighted filter with the density-weighted filter, e.g.

$$\widetilde{\psi_i\psi_j} - \tilde{\psi}_i\tilde{\psi}_j = C_{SS}\left(\widehat{\tilde{\psi}_i\tilde{\psi}_j} - \hat{\tilde{\psi}}_i\hat{\tilde{\psi}}_j\right), \tag{B 2}$$

where re-filtering is always unweighted.

From (A 2)

$$\bar{\psi}_i(\mathbf{x}_0) = \psi_i(\mathbf{x}_0) + \frac{\partial\psi_i}{\partial x_m}(\mathbf{x}_0)\,\overline{(x_m - x_{m_0})} + \frac{\partial^2\psi_i}{\partial x_m\partial x_n}(\mathbf{x}_0)\,\tfrac{1}{2}\overline{(x_m - x_{m_0})(x_n - x_{n_0})} + O\left(\bar{\Delta}^3\right), \tag{B 3}$$

$$\hat{\psi}_i(\mathbf{x}_0) = \psi_i(\mathbf{x}_0) + \frac{\partial\psi_i}{\partial x_m}(\mathbf{x}_0)\,\widehat{(x_m - x_{m_0})} + \frac{\partial^2\psi_i}{\partial x_m\partial x_n}(\mathbf{x}_0)\,\tfrac{1}{2}\widehat{(x_m - x_{m_0})(x_n - x_{n_0})} + O\left(\bar{\Delta}^3\right). \tag{B 4}$$

Then

$$\hat{\bar{\psi}}_i = \bar{\psi}_i(\mathbf{x}_0) + \frac{\partial\bar{\psi}_i}{\partial x_m}(\mathbf{x}_0)\,\widehat{(x_m - x_{m_0})} + \frac{\partial^2\bar{\psi}_i}{\partial x_m\partial x_n}(\mathbf{x}_0)\,\tfrac{1}{2}\widehat{(x_m - x_{m_0})(x_n - x_{n_0})} + O\left(\bar{\Delta}^3\right), \tag{B 5}$$

$$\widehat{\bar{\psi}_i\bar{\psi}_j} = \left(\bar{\psi}_i\bar{\psi}_j\right)(\mathbf{x}_0) + \frac{\partial\left(\bar{\psi}_i\bar{\psi}_j\right)}{\partial x_m}(\mathbf{x}_0)\,\widehat{(x_m - x_{m_0})} + \frac{\partial^2\left(\bar{\psi}_i\bar{\psi}_j\right)}{\partial x_m\partial x_n}(\mathbf{x}_0)\,\tfrac{1}{2}\widehat{(x_m - x_{m_0})(x_n - x_{n_0})} + O\left(\bar{\Delta}^3\right), \tag{B 6}$$

$$\begin{aligned}\hat{\bar{\psi}}_i\hat{\bar{\psi}}_j = {} & \left[\bar{\psi}_i(\mathbf{x}_0) + \frac{\partial\bar{\psi}_i}{\partial x_m}(\mathbf{x}_0)\,\widehat{(x_m - x_{m_0})} + \frac{\partial^2\bar{\psi}_i}{\partial x_m\partial x_n}(\mathbf{x}_0)\,\tfrac{1}{2}\widehat{(x_m - x_{m_0})(x_n - x_{n_0})} + O\left(\bar{\Delta}^3\right)\right] \\ & \times\left[\bar{\psi}_j(\mathbf{x}_0) + \frac{\partial\bar{\psi}_j}{\partial x_k}(\mathbf{x}_0)\,\widehat{(x_k - x_{k_0})} + \frac{\partial^2\bar{\psi}_j}{\partial x_k\partial x_l}(\mathbf{x}_0)\,\tfrac{1}{2}\widehat{(x_k - x_{k_0})(x_l - x_{l_0})} + O\left(\bar{\Delta}^3\right)\right],\end{aligned} \tag{B 7}$$

$$\widehat{\bar{\psi}_i\bar{\psi}_j}-\hat{\bar{\psi}}_i\hat{\bar{\psi}}_j = \frac{\partial\bar{\psi}_i}{\partial x_m}(\mathbf{x}_0)\frac{\partial\bar{\psi}_j}{\partial x_n}(\mathbf{x}_0)\left[\widehat{(x_m - x_{m_0})(x_n - x_{n_0})} - \widehat{(x_m - x_{m_0})}\widehat{(x_n - x_{n_0})}\right] + O\left(\bar{\Delta}^3\right). \tag{B 8}$$

From (B 1)

$$C_{SS} = \frac{\overline{(\psi_i\psi_j - \bar{\psi}_i\bar{\psi}_j)}}{\left(\widehat{\bar{\psi}_i\bar{\psi}_j} - \hat{\bar{\psi}}_i\hat{\bar{\psi}}_j\right)} \text{ if } \left(\widehat{\bar{\psi}_i\bar{\psi}_j} - \hat{\bar{\psi}}_i\hat{\bar{\psi}}_j\right) \neq 0. \tag{B 9}$$

Using (A 5) and (B 8)

$$C_{SS} = \frac{\left(\frac{\partial\psi_i}{\partial x_k}\frac{\partial\psi_j}{\partial x_l}\right)}{\left(\frac{\partial\bar{\psi}_i}{\partial x_m}\frac{\partial\bar{\psi}_j}{\partial x_n}\right)} \frac{\left[\overline{(x_k - x_{k_0})(x_l - x_{l_0})} - \overline{(x_k - x_{k_0})}\overline{(x_l - x_{l_0})}\right]}{\left[\widehat{(x_m - x_{m_0})(x_n - x_{n_0})} - \widehat{(x_m - x_{m_0})}\widehat{(x_n - x_{n_0})}\right]}.$$

For symmetrical filtering volumes $\overline{(x_k - x_{k_0})} = 0$ and $\widehat{(x_m - x_{m_0})} = 0$; then assuming that $\frac{\partial\psi_i}{\partial x_k}\frac{\partial\psi_j}{\partial x_l} \simeq \frac{\partial\bar{\psi}_i}{\partial x_k}\frac{\partial\bar{\psi}_j}{\partial x_l}$ leads to

$$C_{SS} \simeq \frac{\overline{(x_k - x_{k_0})(x_l - x_{l_0})}}{\widehat{(x_m - x_{m_0})(x_n - x_{n_0})}}. \tag{B 10}$$

In the case of a cubic top-hat filter, this would be

$$C_{SS} \simeq \frac{\bar{\Delta}^2}{\hat{\Delta}^2} = \left(\frac{1}{\hat{\Delta}/\bar{\Delta}}\right)^2 \tag{B 11}$$

This analysis shows the dependence of C_{SS} on the test-filter to grid-filter ratio. However, it might not predict C_{SS} because, generally, $\partial\bar{\psi}_i/\partial x_k$ is not a good approximation to $\partial\psi_i/\partial x_k$. (From (A 2) the error in the approximation is proportional to $\partial^2\psi_i/(\partial x_k\partial x_l)$ which is usually not small in a turbulent flow field.)

This work was conducted at the Jet Propulsion Institute (JPL) of the California Institute of Technology (Caltech) under the sponsorship of the U.S. Department of Energy (DOE), with Mr. Neil Rossmeissl (DOE Headquarters) and Mr. D. Hooker (DOE Golden Center) serving as contract monitors, under an agreement with the National Aeronautics and Space Administration.. Computations were performed on the SGI Origin2000 at the JPL Supercomputing Center.

REFERENCES

AYYUB, B. & MCCUEN, R. 1997 *Probability, Statistics and Reliability for Engineers*. Boca Raton, Florida: CRC Press.

BARDINA, J., FERZIGER, J. & REYNOLDS, W. 1980 Improved subgrid scale models for large eddy simulation. *Tech. Rep.* 80-1357. AIAA.

CLARK, R., FERZIGER, J. & REYNOLDS, W. 1979 Evaluation of subgrid-scale models using an accurately simulated turbulent flow. *Journal of Fluid Mechanics* **91** (1), 1–16.

ERLEBACHER, G., HUSSAINI, M., SPEZIALE, C. & ZANG, T. 1992 Toward the large-eddy simulation of compressible turbulent flows. *Journal of Fluid Mechanics* **238**, 155–185.

FUREBY, C. 1996 On subgrid scale modeling in large eddy simulations of compressible fluid flow. *Physics of Fluids A* **8** (5), 1301–1311.

KENNEDY, C. & CARPENTER, M. 1994 Several new numerical methods for compressible shear layer simulations. *Applied Numerical Mathematics* **14**, 397–433.

LIU, S., MENEVEAU, C. & KATZ, J. 1994 On the properties of similarity subgrid-scale models as deduced from measurements in a turbulent jet. *Journal of Fluid Mechanics* **275**, 83–119.

MARTIN, M., PIOMELLI, U. & CANDLER, G. 2000 Subgrid-scale models for compressible large-eddy simulations. *Theoretical and Computational Fluid Dynamics* **13** (5), 361–376.

MILLER, R. & BELLAN, J. 1999 Direct numerical simulation of a confined three-dimensional gas mixing layer with one evaporating hydrocarbon-droplet laden stream. *Journal of Fluid Mechanics* **384**, 293–338.

MILLER, R. & BELLAN, J. 2000 Direct numerical simulation and subgrid analysis of a transitional droplet laden mixing layer. *Physics of Fluids* **12** (3), 650–671.

MOSER, R. & ROGERS, M. 1991 Mixing transition and the cascade to small scales in a plane mixing layer. *Physics of Fluids A* **3** (5), 1128–1134.

OKONG'O, N. & BELLAN, J. 2000 A priori subgrid analysis of temporal mixing layers with evaporating droplets. *Physics of Fluids* **12** (6), 1573–1591.

OKONG'O, N. & BELLAN, J. 2002 Consistent large eddy simulation of a temporal mixing layer laden with evaporating drops. Part I: Direct numerical simulation and formulation Submitted to Journal of Fluid Mechanics.

POINSOT, T. & LELE, S. 1992 Boundary conditions for direct simulations of compressible viscous flows. *Journal of Computational Physics* **101**, 104–129.

PRUETT, C. & ADAMS, N. 2000 *A priori* analyses of three subgrid-scale models for one-parameter families of filters. *Physics of Fluids* **12** (5), 1133–1142.

PRUETT, C., SOCHACKI, J. & ADAMS, N. 2001 On Taylor-series expansions of residual stress. *Physics of Fluids* **13** (9), 2578–2589.

SMAGORINKSY, J. 1993 Some historical remarks on the use of nonlinear viscosities. In *Large Eddy Simulation of Complex Engineering and Geophysical Flows* (ed. B. Galperin & S. Orszag), chap. 1, pp. 3–36. Cambridge University Press.

VREMAN, B., GEURTS, B. & KUERTEN, H. 1997 Large-eddy simulation of the turbulent mixing layer. *Journal of Fluid Mechanics* **339**, 357–390.

WILLIAMS, F. 1965 *Combustion Theory*. Addison-Wesley.

YOSHIZAWA, A. 1986 Statistical theory for compressible turbulent shear flows, with the application to subgrid modeling. *Physics of Fluids* **29** (7), 2152–2164.

Run	Re_0	ML_0	N_d	$N_1 \times N_2 \times N_3$	t^*_{trans}	$\delta_m/\delta_{\omega,0}$ at t^*_{trans}	Re_m at t^*_{trans}	CPU-hours (estimated)
SP500	500	0	0	256×288×160	100	2.580	1290	688
TP500a2	500	0.2	2277222	256×288×160	100	2.827	1414	1336
TP500a5	500	0.5	5693055	256×288×160	105	2.722	1361	2075
SP600	600	0	0	288×320×176	100	2.485	1491	1054
TP600a2	600	0.2	2993630	288×320×176	105	2.627	1576	2252
TP600a5	600	0.5	7484075	288×320×176	105	2.794	1676	3070

Re_0: initial-vorticity-thickness Reynolds number, $\mathrm{Re}_0 = \rho_0 \Delta U_0 \delta_{\omega,0}/\mu$

ML_0: initial mass loading

N_d: initial number of drops

N_1, N_2, N_3: number of grid points in x_1, x_2 and x_3 directions respectively

t^*_{trans}: transition time (dimensionless), $t^* = t\Delta U_0/\delta_{\omega,0}$

Re_m: momentum-thickness Reynolds number, $\mathrm{Re}_m = \rho_0 \Delta U_0 \delta_m/\mu$

CPU hours are estimates on 64 processors of an SGI Origin2000

For all cases: L_1=0.2m, L_2=0.22m, L_3=0.12m , $M_{c,0}$=0.35, $T_{C,0}$=375K, ρ_0=0.9415kg/m^3, ΔU_0=271.7m/s, $\delta_{\omega,0}$=6.859×10^{-3}m.

For drop laden cases: $T_{d,0}$=345K, ρ_L=642kg/m^3, the initial St has a Gaussian distribution with mean 3 and standard deviation 0.5.

TABLE 1. Initial conditions and transition times.

	$\bar{\Delta} = 4\Delta x$			$\bar{\Delta} = 8\Delta x$		
Model	Baseline	Random	Deterministic	Baseline	Random	Deterministic
$u_{1,f}$	1.002	0.999	1.002	1.005	0.998	1.004
$u_{2,f}$	1.020	0.967	1.018	1.041	0.913	1.031
$u_{3,f}$	1.076	0.890	1.063	1.175	0.712	1.092
T_f	0.999	0.999	0.999	0.999	0.998	0.999
$Y_{V,f}$	1.006	1.003	1.006	1.014	1.008	1.013
p_f	1.000	1.000	1.000	1.001	1.001	1.001

TABLE 2. Slopes from least squares fit of exact to modeled quantities, slope=exact/model, TP600a2 at t^*=105: Unfiltered primitive variables interpolated to drop locations.

	$\bar{\Delta} = 4\Delta x$			$\bar{\Delta} = 8\Delta x$		
Model	Baseline	Random	Deterministic	Baseline	Random	Deterministic
$S_{I,d}$	0.949	0.847	0.944	0.869	0.729	0.853
$S_{II,1,d}$	0.839	0.440	0.803	0.556	0.229	0.514
$S_{II,2,d}$	0.843	0.355	0.795	0.498	0.156	0.424
$S_{II,3,d}$	0.787	0.288	0.718	0.390	0.113	0.306
$S_{III,d}$	0.948	0.798	0.942	0.864	0.669	0.852

TABLE 3. Slopes from least squares fit of exact to modeled quantities, slope=exact/model, TP600a2 at t^*=105: Drop source terms.

	$\bar{\Delta} = 4\Delta x$			$\bar{\Delta} = 8\Delta x$		
Model	Baseline	Random	Deterministic	Baseline	Random	Deterministic
$\bar{S}_I$	0.879	0.855	0.878	0.752	0.726	0.749
$\bar{S}_{II,1}$	0.824	0.787	0.806	0.610	0.583	0.592
$\bar{S}_{II,2}$	0.866	0.814	0.852	0.619	0.585	0.592
$\bar{S}_{II,3}$	0.813	0.745	0.786	0.447	0.445	0.428
$\bar{S}_{III}$	0.872	0.844	0.870	0.738	0.711	0.733

TABLE 4. Slopes from least squares fit of exact to modeled quantities, slope=exact/model, TP600a2 at t^*=105: Filtered source terms.

SGS quantity	SP600	TP600a2	SP600	TP600a2
	$\bar{\Delta} = 4\Delta x$	$\bar{\Delta} = 4\Delta x$	$\bar{\Delta} = 8\Delta x$	$\bar{\Delta} = 8\Delta x$
$\bar{\rho}\,(\tau_{11} - \tau_{kk}/3)$	0.0513	0.0478	0.0500	0.0456
$\bar{\rho}\,(\tau_{22} - \tau_{kk}/3)$	0.0366	0.0362	0.0280	0.0304
$\bar{\rho}\,(\tau_{33} - \tau_{kk}/3)$	0.0396	0.0400	0.0403	0.0414
$\bar{\rho}\tau_{12}$	0.0681	0.0660	0.0710	0.0733
$\bar{\rho}\tau_{13}$	0.0450	0.0436	0.0370	0.0399
$\bar{\rho}\tau_{23}$	0.0325	0.0340	0.0284	0.0272
$\bar{\rho}\zeta_1$	0.0885	0.1464	0.0486	0.1375
$\bar{\rho}\zeta_2$	0.1121	0.1505	0.1004	0.1576
$\bar{\rho}\zeta_3$	0.0925	0.0873	0.0752	0.0757
$\bar{\rho}\eta_1$	–	0.1512	–	0.1464
$\bar{\rho}\eta_2$	–	0.1536	–	0.1598
$\bar{\rho}\eta_3$	–	0.0884	–	0.0763
Average slope	0.0629	0.0871	0.0532	0.0843
Std. Dev. of slopes	0.0287	0.0501	0.0243	0.0518
Average correlation	0.25	0.31	0.24	0.31

TABLE 5. Slopes from least squares fit of SGS quantities to SGS models, Smagorinsky model.

	SP600	SP600	TP600a2	TP600a2
	$\bar{\Delta} = 4\Delta x$	$\bar{\Delta} = 8\Delta x$	$\bar{\Delta} = 4\Delta x$	$\bar{\Delta} = 8\Delta x$
Slope	0.3043	0.3154	0.3096	0.3265
Correlation	0.81	0.79	0.79	0.77

TABLE 6. Slopes from least squares fit of SGS quantities to SGS models, Yoshizawa model for $\bar{\rho}\tau_{kk}$.

SGS quantity	SP600	TP600a2	SP600	TP600a2
	$\bar{\Delta} = 4\Delta x$	$\bar{\Delta} = 4\Delta x$	$\bar{\Delta} = 8\Delta x$	$\bar{\Delta} = 8\Delta x$
$\bar{\rho}\tau_{11}$	0.1596	0.1655	0.1556	0.1629
$\bar{\rho}\tau_{22}$	0.1645	0.1683	0.1694	0.1756
$\bar{\rho}\tau_{33}$	0.1683	0.1723	0.1820	0.1870
$\bar{\rho}\tau_{12}$	0.1448	0.1478	0.1313	0.1339
$\bar{\rho}\tau_{13}$	0.1479	0.1506	0.1334	0.1354
$\bar{\rho}\tau_{23}$	0.1475	0.1503	0.1343	0.1367
$\bar{\rho}\zeta_1$	0.1488	0.1464	0.1346	0.1345
$\bar{\rho}\zeta_2$	0.1475	0.1450	0.1338	0.1324
$\bar{\rho}\zeta_3$	0.1489	0.1463	0.1334	0.1319
$\bar{\rho}\eta_1$	–	0.1468	–	0.1346
$\bar{\rho}\eta_2$	–	0.1455	–	0.1327
$\bar{\rho}\eta_3$	–	0.1466	–	0.1322
$\sigma^2_{SGS}\left(\tilde{T}\right)$	0.1737	0.1758	0.1809	0.1828
$\sigma^2_{SGS}\left(\tilde{Y}_V\right)$	–	0.1725	–	0.1784
$\sigma^2_{SGS}\left(\bar{p}\right)$	0.1588	0.1666	0.1349	0.1580
Average slope	0.1552	0.1564	0.1476	0.1499
Std. dev. of slopes	0.0099	0.0119	0.0205	0.0216
Average correlation	0.97	0.97	0.92	0.91

TABLE 7. Slopes from least squares fit of SGS quantities to SGS models, Gradient model.

SGS quantity	SP600	TP600a2	SP600	TP600a2
	$\bar{\Delta} = 4\Delta x$	$\bar{\Delta} = 4\Delta x$	$\bar{\Delta} = 8\Delta x$	$\bar{\Delta} = 8\Delta x$
$\bar{\rho}\tau_{11}$	1.5832	1.6691	1.9327	2.0636
$\bar{\rho}\tau_{22}$	1.6733	1.7390	2.2583	2.3869
$\bar{\rho}\tau_{33}$	1.7341	1.7954	2.5860	2.6523
$\bar{\rho}\tau_{12}$	1.4629	1.5364	1.6903	1.7806
$\bar{\rho}\tau_{13}$	1.5728	1.6212	1.9217	1.9603
$\bar{\rho}\tau_{23}$	1.5864	1.6472	1.9940	2.0627
$\bar{\rho}\zeta_1$	1.5317	1.4812	1.7572	1.7383
$\bar{\rho}\zeta_2$	1.5340	1.4754	1.7675	1.7472
$\bar{\rho}\zeta_3$	1.6009	1.5378	1.9138	1.8865
$\bar{\rho}\eta_1$	–	1.4888	–	1.7480
$\bar{\rho}\eta_2$	–	1.4850	–	1.7581
$\bar{\rho}\eta_3$	–	1.5422	–	1.8929
$\sigma^2_{SGS}\left(\tilde{T}\right)$	1.8006	1.8430	2.3777	2.4825
$\sigma^2_{SGS}\left(\tilde{Y}_V\right)$	–	1.7918	–	2.4081
$\sigma^2_{SGS}\left(\bar{p}\right)$	1.4381	1.6450	1.4324	1.8154
Average slope	1.5925	1.6199	1.9665	2.0256
Std. dev. of slopes	0.1087	0.1263	0.3301	0.3088
Average correlation	0.94	0.93	0.89	0.88

TABLE 8. Slopes from least squares fit of SGS quantities to SGS models, Similarity model with $\hat{\Delta} = \bar{\Delta}$.

SGS quantity	SP600	TP600a2	SP600	TP600a2
	$\bar{\Delta} = 4\Delta x$	$\bar{\Delta} = 4\Delta x$	$\bar{\Delta} = 8\Delta x$	$\bar{\Delta} = 8\Delta x$
$\bar{\rho}\tau_{11}$	0.6114	0.6562	0.7143	0.7818
$\bar{\rho}\tau_{22}$	0.6780	0.7163	0.9460	1.0100
$\bar{\rho}\tau_{33}$	0.7317	0.7613	1.2425	1.2588
$\bar{\rho}\tau_{12}$	0.5508	0.5949	0.6384	0.6679
$\bar{\rho}\tau_{13}$	0.6522	0.6744	0.8130	0.8180
$\bar{\rho}\tau_{23}$	0.6678	0.7052	0.8991	0.9187
$\bar{\rho}\zeta_1$	0.5921	0.5638	0.6444	0.6509
$\bar{\rho}\zeta_2$	0.5969	0.5625	0.6438	0.6819
$\bar{\rho}\zeta_3$	0.6611	0.6236	0.7833	0.8002
$\bar{\rho}\eta_1$	–	0.5683	–	0.6565
$\bar{\rho}\eta_2$	–	0.5676	–	0.6897
$\bar{\rho}\eta_3$	–	0.6248	–	0.8049
$\sigma^2_{SGS}\left(\tilde{T}\right)$	0.7412	0.7719	0.9442	1.0575
$\sigma^2_{SGS}\left(\tilde{Y}_V\right)$	–	0.7439	–	1.0229
$\sigma^2_{SGS}\left(\bar{p}\right)$	0.4913	0.6211	0.4246	0.5668
Average slope	0.6340	0.6504	0.7903	0.8259
Std. dev. of slopes	0.0749	0.0746	0.2168	0.1919
Average correlation	0.82	0.82	0.74	0.73

TABLE 9. Slopes from least squares fit of SGS quantities to SGS models, Similarity model with $\hat{\Delta} = 2\bar{\Delta}$.

SGS Model	SP600	TP600a2	Average slopes equal?
	$\bar{\Delta}/\Delta x = 4$	$\bar{\Delta}/\Delta x = 4$	
Smagorinsky	0.0629	0.0871	yes
Gradient	0.1552	0.1564	yes
Similarity ($\hat{\Delta} = \bar{\Delta}$)	1.5925	1.6199	yes
Similarity ($\hat{\Delta} = 2\bar{\Delta}$)	0.6340	0.6504	yes

TABLE 10. Average slopes and t-Test for equality of average slopes, $\bar{\Delta} = 4\Delta x$.

SGS Model	SP600	TP600a2	Average slopes equal?
	$\bar{\Delta}/\Delta x = 8$	$\bar{\Delta}/\Delta x = 8$	
Smagorinsky	0.0532	0.0843	yes
Gradient	0.1476	0.1499	yes
Similarity ($\hat{\Delta} = \bar{\Delta}$)	1.9665	2.0256	yes
Similarity ($\hat{\Delta} = 2\bar{\Delta}$)	0.7903	0.8259	yes

TABLE 11. Average slopes and t-test for equality of average slopes, $\bar{\Delta} = 8\Delta x$.

SGS Model	SP600	SP600	Average slopes equal?
	$\bar{\Delta}/\Delta x = 4$	$\bar{\Delta}/\Delta x = 8$	
Smagorinsky	0.0629	0.0532	yes
Gradient	0.1514	0.1532	yes
Similarity ($\hat{\Delta} = \bar{\Delta}$)	1.5925	1.9665	no
Similarity ($\hat{\Delta} = 2\bar{\Delta}$)	0.6340	0.7903	no

TABLE 12. Average slopes and t-test for equality of average slopes, SP600.

SGS Model	TP600a2	TP600a2	Average slopes equal?
	$\bar{\Delta}/\Delta x = 4$	$\bar{\Delta}/\Delta x = 8$	
Smagorinsky	0.0871	0.0843	yes
Gradient	0.1564	0.1499	yes
Similarity ($\hat{\Delta} = \bar{\Delta}$)	1.6199	2.0256	no
Similarity ($\hat{\Delta} = 2\bar{\Delta}$)	0.6504	0.8259	no

TABLE 13. Average slopes and t-test for equality of avearage slopes, TP600a2.

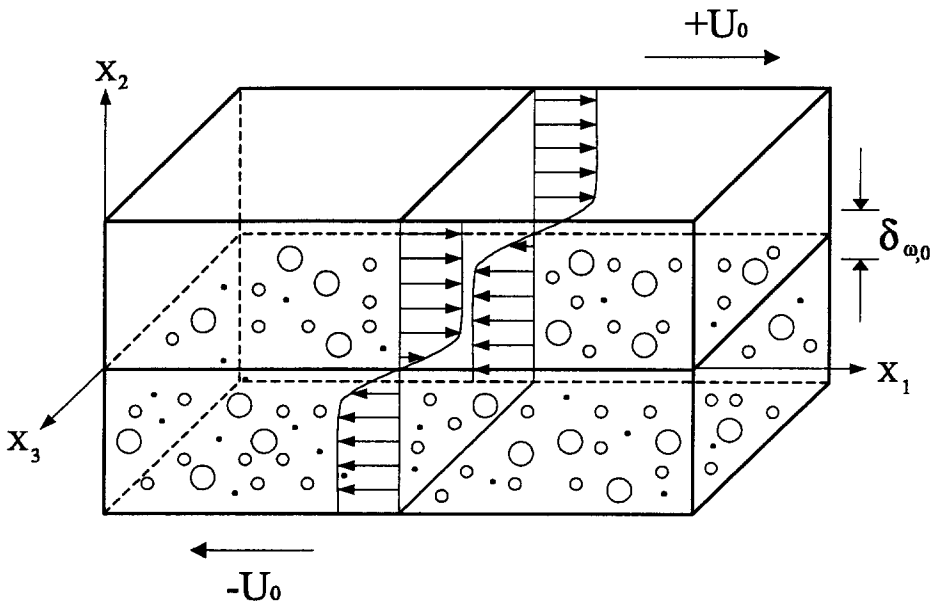

FIGURE 1. Mixing layer configuration

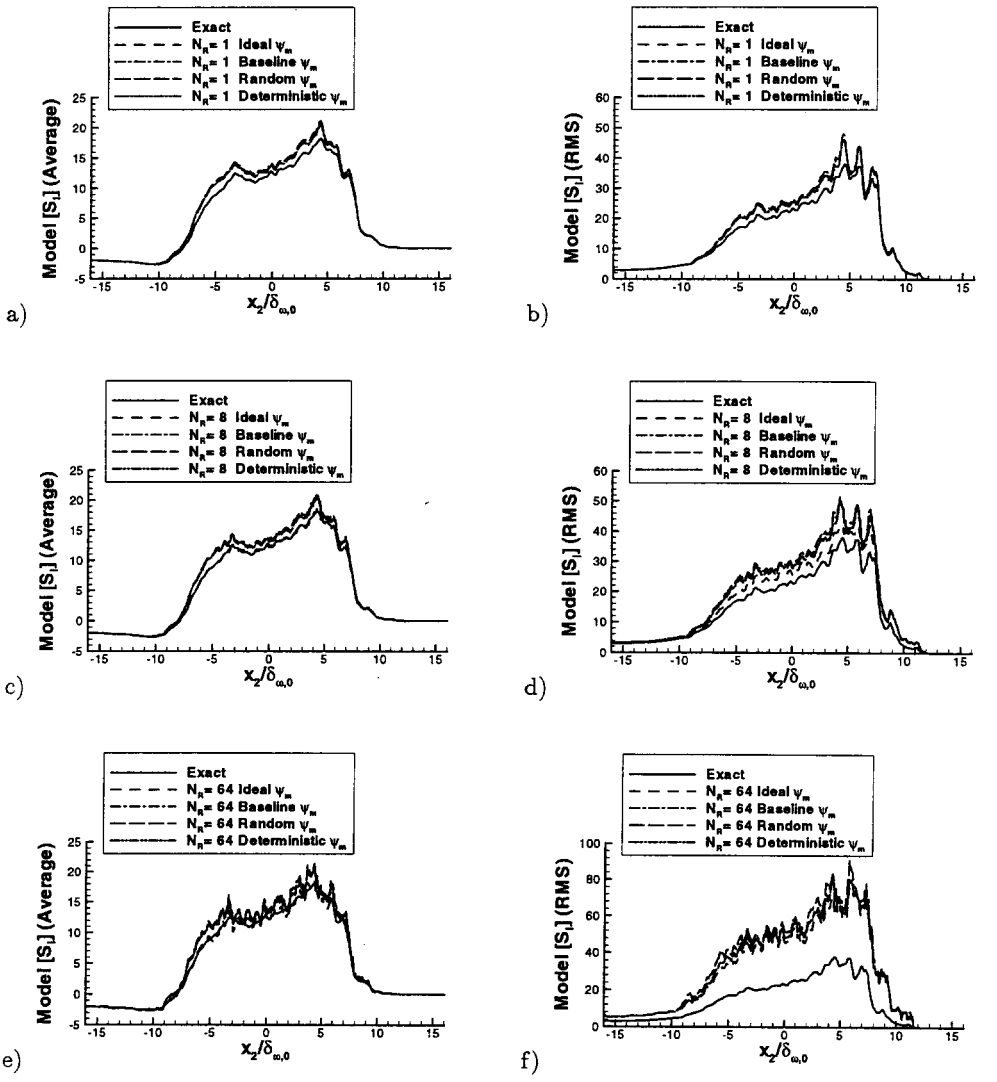

FIGURE 2. Homogeneous (x_1, x_3) plane (a,c,e) averages and (b,d,f) RMS of $\bar{S}_I$ models, TP600a2 at t^*=105, $\bar{\Delta}$=4Δx: (a,b) N_R=1, (c,d) N_R=8, (e,f) N_R=64. The filtered source term models are designated ideal, baseline, random or deterministic according to ψ_m, the model used for the unfiltered gas-phase variables. N_R is the ratio of the number of actual drops to the number of computational drops. (In the figures, the notations [S] and Δ are used for $\bar{S}$ and $\bar{\Delta}$ respectively.)

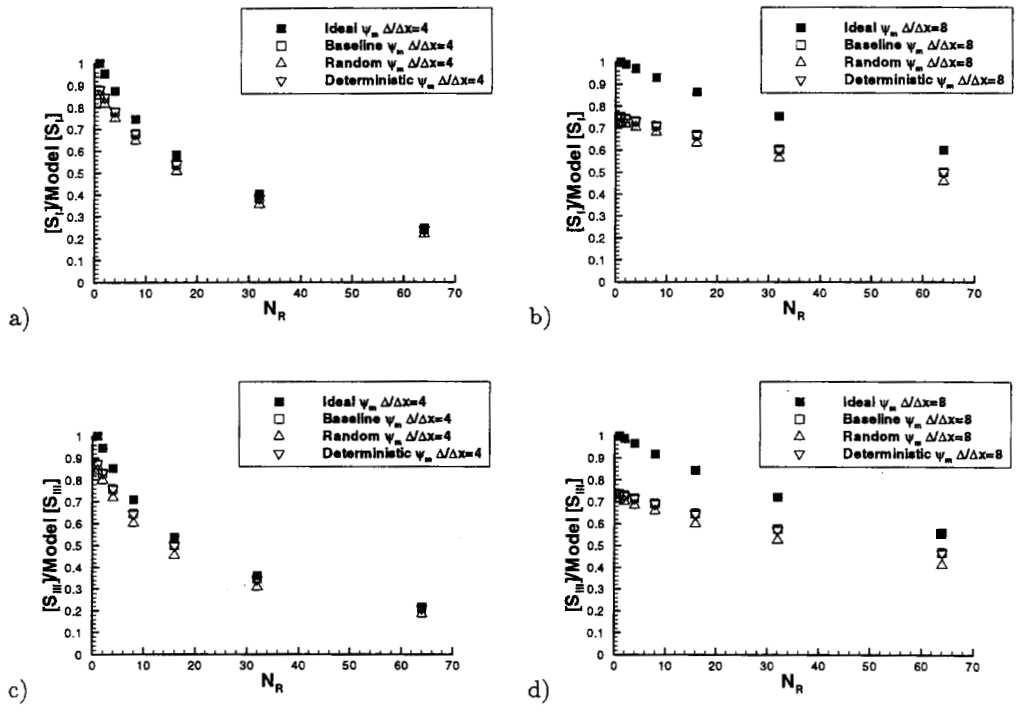

FIGURE 3. Slopes from least squares fit of exact to modeled filtered source terms, TP600a2 at t^*=105: (a,b) $\bar{S}_I$, (c,d) $\bar{S}_{III}$, for (a,c) $\bar{\Delta} = 4\Delta x$ and (b,d) $\bar{\Delta} = 8\Delta x$. See caption of figure 2 for additional information.

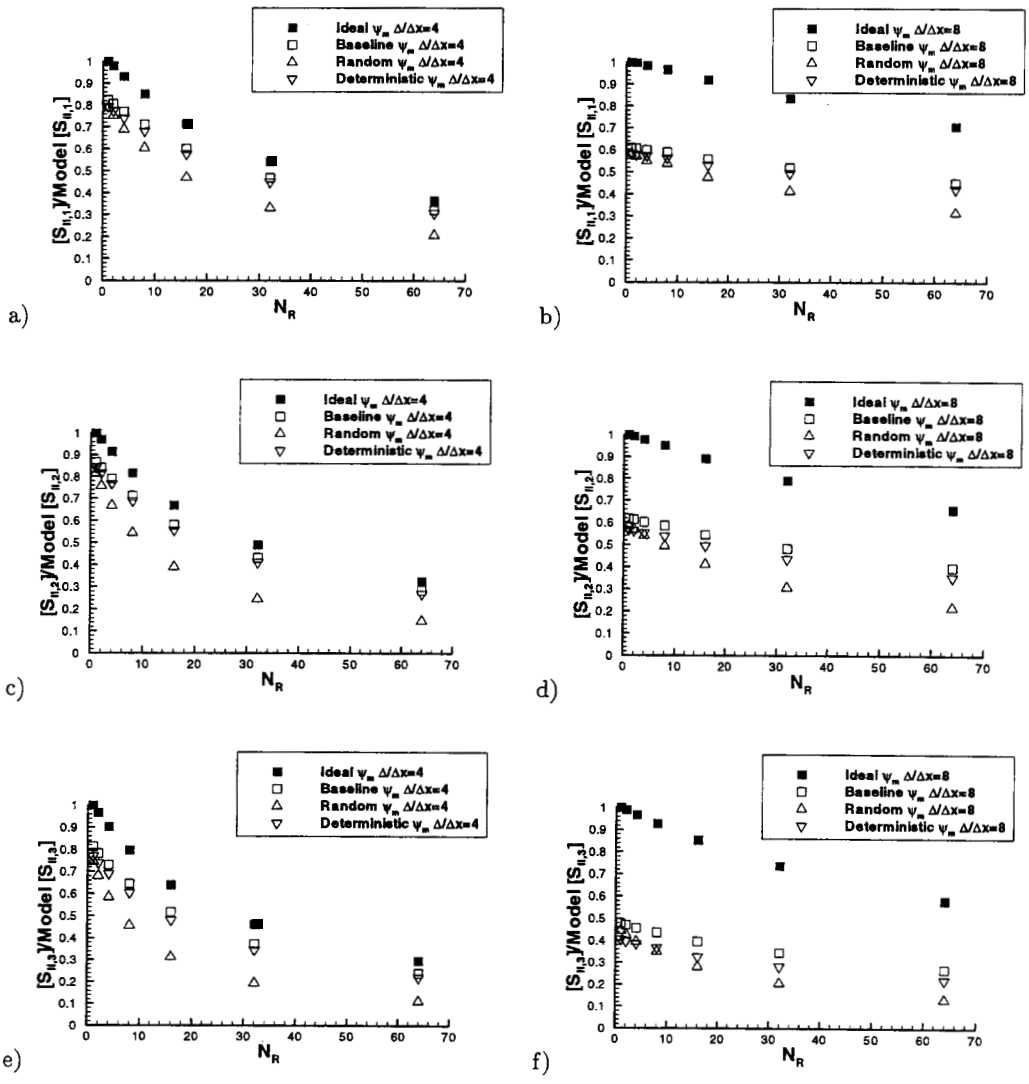

FIGURE 4. As for figure 3: (a,b) $\bar{S}_{II,1}$, (c,d) $\bar{S}_{II,2}$, (e,f) $\bar{S}_{II,3}$ for (a,c,e) $\bar{\Delta} = 4\Delta x$ and (b,d,f) $\bar{\Delta} = 8\Delta x$.

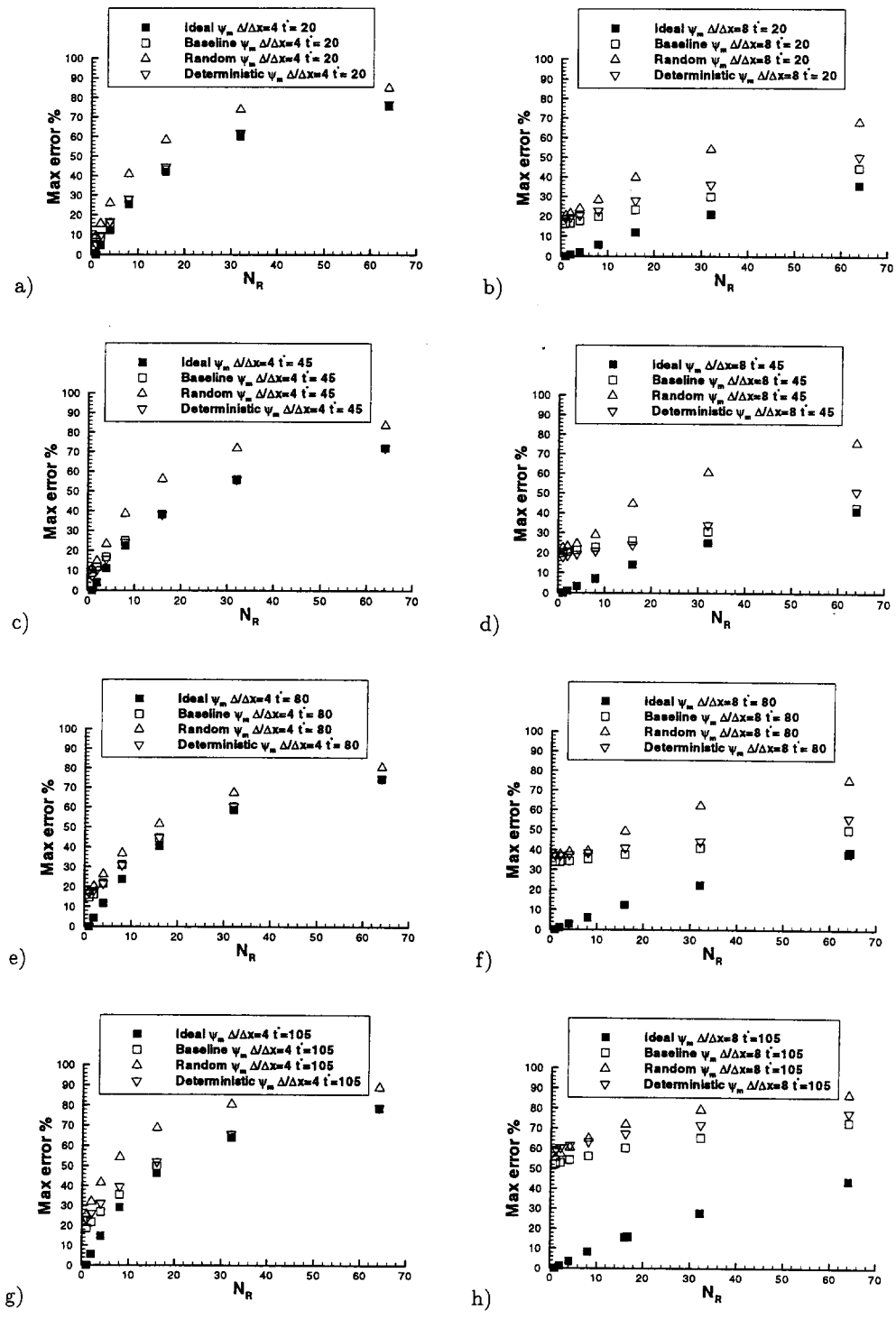

FIGURE 5. Maximal percentage error in filtered source term models, TP600a2 at: (a,b) t^*=20, (c,d) t^*= 45, (e,f) t^*=80, (g,h) t^*= 105 for (a,c,e,g) $\bar{\Delta} = 4\Delta x$ and (b,d,f,h) $\bar{\Delta} = 8\Delta x$. See caption of figure 2 for additional information.